

KRAFTY: Khatri-Rao Framework for Joint Cluster Recovery

BY SIYI GAO

*Department of Statistics, University of Virginia
Charlottesville, VA 22904, USA
sg7nx@virginia.edu*

ZACHARY LUBBERTS

*Department of Statistics, University of Virginia
Charlottesville, VA 22904, USA
zlubberts@virginia.edu*

MARIANNA PENSKY

*Department of Mathematics, University of Central Florida
Orlando, FL 32816, USA
Marianna.Pensky@ucf.edu*

SUMMARY

When multiple datasets describe complementary information about the same set of entities, for example, brain scans of an individual over time, global trade network across years, or user information across social media platforms, integrating these snapshots allows us to see a more holistic picture. A common way of identifying structure in data is through clustering, but while clustering may be applied to each dataset separately, we learn more in the multi-view setting by identifying joint clusters. We consider a clustering problem where each view conflates some of these joint clusters, only revealing partial information, and seek to recover the true joint cluster structure. We introduce this multi-view clustering model and a method for recovering it: the transposed Khatri–RAo Framework for joint cluster recovery (KRAFTY). The model is flexible and can accommodate a variety of data-generating processes, including latent positions in random dot product graphs and Gaussian mixtures. A key advantage of KRAFTY is that it represents joint clusters in a space with sufficient dimension so that each joint cluster occupies an orthogonal subspace in the transposed Khatri-Rao matrix, which results in a sharp drop in the scree plot at the true number of joint clusters, enabling easy model selection. Our simulations show that when the number of joint clusters exceeds the sum of the numbers of clusters in each individual view, our method outperforms existing methods in both joint clustering accuracy and estimation of the number of joint clusters.

Some key words: Community detection; Khatri-Rao product; Multi-view clustering

1. INTRODUCTION

1.1. *Background and Motivation*

Community detection and clustering are core tasks in statistics and machine learning Jaeger & Banks (2023); Milligan & Cooper (1987); Abbe (2023); Fortunato & Newman (2022). Clustering

analysis is defined as partitioning objects into groups (clusters) so that within-group similarity is high and between-group similarity is low; similarity may be defined by network connectivity, feature-space distances, or other affinities Jaeger & Banks (2023); Milligan & Cooper (1987); von Luxburg (2007). Cluster analysis has been applied to data in several modern applications, such as genetic profiles Toh & Horimoto (2002) and social-network snapshots Handcock et al. (2007), to uncover meaningful latent patterns, and numerous techniques have been developed for single-dataset clustering Jaeger & Banks (2023); Milligan & Cooper (1987); von Luxburg (2007); Jin et al. (2023).

Early work in the multi-view setting focused on recovery of a single, consistent clustering across sources Abbe (2023); Fortunato & Newman (2022); Jin et al. (2023). More recently, multi-view clustering has gained attention Yang & Wang (2018); Vallès-Català et al. (2016) as many applications provide datasets from different sources or views, and joint clustering can yield a more informative partition. There has also been a growing interest in studying differences between subspaces across networks or clusterings MacDonald et al. (2021); Gallagher et al. (2021); Arroyo et al. (2020); Agterberg et al. (2025), leading to numerous multi-view spectral clustering approaches Jing et al. (2021); Lei & Lin (2023). A common multi-view spectral approach concatenates the per-view spectral embeddings and then performs a second spectral decomposition followed by clustering, called Multiple Adjacency Spectral Embedding (**MASE**) in Arroyo et al. (2020). Such approaches have two drawbacks. First, rank deficiency: each view’s embedding dimension is typically set to its own number of clusters, so concatenation yields a space of dimension at most the sum of per-view cluster counts, whereas the true number of joint clusters can be as large as the product across views. Second, determining the number of joint clusters: these methods usually lack an explicit estimator for the joint number of clusters, relying instead on an “elbow” in the scree plot, which may be ambiguous. To address these challenges, our study introduces the transposed Khatri-Rao product framework, which provides sufficient rank for estimating the number of joint clusters and achieves strong performance in both estimating the number of joint clusters and joint clustering.

1.2. Notations

For a positive integer n , we denote $[n] = \{1, \dots, n\}$. We denote by $\mathcal{O}_{r,k}$ the set of $r \times k$ matrices with orthonormal columns, where $\mathcal{O}_r = \mathcal{O}_{r,r}$. We denote the set of clustering matrices that partition n objects into K clusters by $\mathcal{C}_{n,K}$. Here, $\mathcal{C}_{n,K}$ consists of $n \times K$ binary matrices where each row has one value 1 and the rest are zeros. We denote the i -th row and the j -th column of a matrix A by, respectively, $A(i, \cdot)$ and $A(\cdot, j)$. We denote the identity matrix of order m by I_m . We denote the matrix of K left singular vectors of matrix X by $\text{SVD}_K(X)$. We denote the Frobenius, spectral, and $2 \rightarrow \infty$ matrix norms by, respectively, $\|\cdot\|_F$, $\|\cdot\|$ and $\|\cdot\|_{2,\infty}$, where $\|A\|_{2,\infty} = \max_i \|A(i, \cdot)\|$. We denote the Hadamard and the Kronecker products of matrices A and B by, respectively, $A \circ B$ and $A \otimes B$. For matrices $A \in \mathbb{R}^{n \times m}$ and $B \in \mathbb{R}^{n \times q}$ with the same number of rows, we define the transposed-Khatri-Rao product as $A \textcircled{\otimes} B \in \mathbb{R}^{n \times mq}$, where for $i \in [n]$,

$$(A \textcircled{\otimes} B)(i, \cdot) = A(i, \cdot) \otimes B(i, \cdot) = [A(i, 1)B(i, \cdot) \mid \dots \mid A(i, m)B(i, \cdot)].$$

Some properties of this product are provided in Appendix A.6. We use C_τ for a generic constant that depends on τ only and can take different values throughout the paper.

1.3. The Model

In this paper, we consider the common scenario where data are obtained from V sources (views). Each of these V views is associated with a clustering assignment $z_v : [n] \rightarrow K_v$ with associated clustering matrix $Z_v \in \{0, 1\}^{n \times K_v}$, where K_v is the number of clusters in view $v \in [V]$.

These clustering assignments may have any joint configuration. Our goal is to recover the joint clustering assignment function $z : [n] \rightarrow [K]$ or associated clustering matrix $Z \in \{0, 1\}^{n \times K}$ that describes the joint configuration of clusters. To make this precise, let the total number of clusters K in the joint assignment be a value

$$\max_{v \in [V]} K_v \leq K \leq \prod_v K_v, \quad (1)$$

and let $Z \in \{0, 1\}^{n \times K}$ be the true joint clustering matrix, which has exactly one nonzero entry in each row. The individual clustering matrices $Z_v = ZP_v$, where $P_v \in \{0, 1\}^{K \times K_v}$ has at least one nonzero entry in each column, and exactly one nonzero entry in each row. This ensures that all of the individual clusterings are consistent with the joint clustering, but may combine some of the joint clusters together. Typically, all views will have fewer clusters individually than the true number of joint clusters.

In what follows, we assume that V is small and data consist of either view-specific estimated clustering matrices $\tilde{Z}_v \in C_{n, K_v}$, $v \in [V]$, or estimated matrices of singular vectors $\tilde{U}_v \in O_{n, K_v}$, $v \in [V]$, that can be used for clustering. We make no additional assumptions on the sources of the data, however, a common scenario would be the results of k -means applied to the V different views.

While the problem initially seems easy, in reality, it is not. Consider a simple situation where $V = 2$. Let $K_1 = K_2 = 3$, let n be large, and let clusters in both views be generated uniformly at random with probability $1/3$. Then, the clustering assignments z_1 and z_2 are independent and the combined clustering consists of $K_1 \times K_2 = 9$ groups of almost equal sizes. If one uses a concatenated matrix $\tilde{Z} = [Z^{(1)} | Z^{(2)}] \in \{0, 1\}^{n \times 6}$, where $Z^{(1)}, Z^{(2)}$ are individual clustering matrices, as a basis for joint clustering, then $\text{rank}(\tilde{Z}) = 5$. For example, if $n = 1000$, the singular values of \tilde{Z} are (25.8852, 18.7956, 18.5849, 18.2198, 17.3010, 0). Hence, the matrix \tilde{Z} is rank-deficient, and it is highly non-trivial to choose the number of clusters in the joint assignment.

As a remedy, here we propose to replace \tilde{Z} by the matrix $Z^{(1,2)} = Z^{(1)} \circledast Z^{(2)}$. It is easy to notice that matrix $Z^{(1,2)} \in C_{n, K_1 K_2}$, so it is a clustering matrix and it has 9 almost identical singular values (11.1803, 11.0454, 10.9087, 10.7238, 10.6301, 10.5830, 10.3923, 9.8489, 9.4340). We shall show later that, in general, the rank of matrix $Z^{(1,2)}$ can be used as a proxy for the number of clusters in the joint assignment, and its estimated version (as well as its version based on estimated matrices of singular values) forms a solid foundation for the recovery of the combined clustering assignment.

As such, our paper introduces the transposed Khatri-RAo Framework for joint cluster recovery (KRAFTY). A key advantage of KRAFTY is that it represents joint clusters in a space with sufficient dimension, which enables more reliable estimation of the number of joint clusters. Figure 1 illustrates the key idea behind application of the transposed Khatri-Rao product. Here, $Z^{(1)}$ and $Z^{(2)}$ are clustering matrices for two datasets over the same set of entities. In this example, $V = 2$ and both views have $K_1 = K_2 = 3$ clusters. Cluster 1 is common for both views while elements of clusters 2 and 3 in the view 1 can be scattered among clusters 2 and 3 in the view 2. This leads to a joint configuration with $K = 5$ different clusters. Matrix $Z^{(1,2)} = Z^{(1)} \circledast Z^{(2)}$ has $3 \times 3 = 9$ columns, where the column indexed by (k_1, k_2) , corresponds to the combination of clusters k_1 and k_2 in the views 1 and 2, respectively. It is easy to see that the only non-zero columns of $Z^{(1,2)}$ correspond to the non-empty combinations of clusters, so that it has 4 zero columns. Again, if $n = 1000$, matrix $Z^{(1,2)}$ has 5 large singular values (18.7617, 13.1149, 12.8452, 12.4900, 12.4499), followed by 4 zeros.

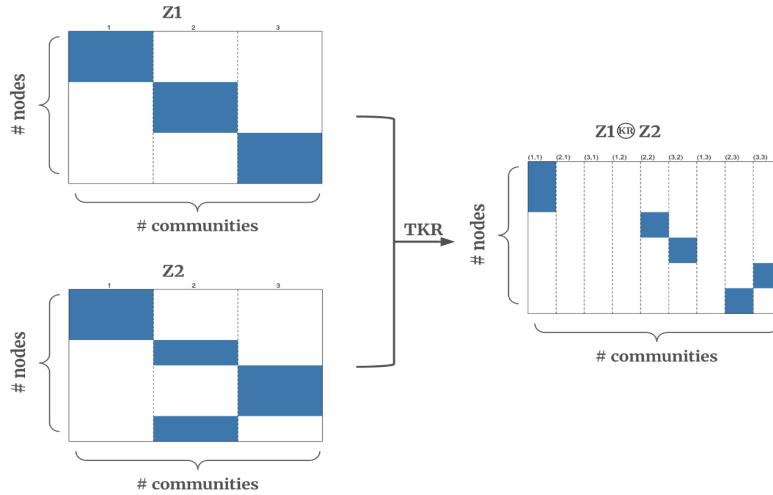


Fig. 1: Graphical illustration of the intuition behind the transposed Khatri-Rao product.

1.4. Related Work

In recent years, community-based statistical models have gained significant attention because they treat clusters not merely as features of the data, but as the generative mechanism behind it Fortunato & Newman (2022). Prominent examples include Gaussian mixture models (GMMs) and the stochastic block model (SBM) Holland et al. (1983). These models have led to a rich literature on community detection in single dataset Abbe (2023); Fortunato & Newman (2022), and a collection of spectral clustering methods (Jin (2015); von Luxburg (2007); Qin & Rohe (2013); Rohe et al. (2011); Lei & Lin (2023); Löffler et al. (2020)). The core idea is to use a matrix factorization, such as the eigen-decomposition or singular value decomposition, to extract a lower-dimensional embedding, which is then clustered using methods such as k -means or hierarchical clustering von Luxburg (2007). These methods perform well in practice and have strong theoretical guarantees: under suitable conditions they are consistent, and can even achieve perfect clustering (Lei & Rinaldo (2015); Lyzinski et al. (2015); Löffler et al. (2020); Pensky (2024); Sussman et al. (2012)). Our method builds on the nice properties of single-source spectral clustering by exploiting the spectral embeddings from each data set.

Moving to multiview clustering, a number of recent studies have been conducted in the multilayer SBM framework (Vallès-Català et al. (2016)). Several clustering methods have been developed, including spectral clustering methods (Jing et al. (2021); Lei & Lin (2023); Agterberg et al. (2025); Domenico et al. (2014); Han et al. (2015)) and matrix factorization (Paul & Chen (2018)). Many methods involve obtaining spectral embeddings from each graph and then concatenating them for a subsequent spectral decomposition, as in MASE Arroyo et al. (2020) and UASE Gallagher et al. (2021). However, these side-by-side concatenation face limitations when the number of joint clusters exceeds the sum of the per-layer cluster counts: because each layer’s embedding dimension is typically set to its own number of clusters, the maximum rank of the concatenated matrix is at most that sum, so the representation can become rank-deficient and fail to capture the full joint structure. Another important line of work is to estimate the number of clusters in multi-view data. Existing methods often rely on visual inspection of the scree-plot “elbow” (Ledesma et al. (2015)) or the automatic dimension selection method by Zhu & Ghodsi (2006). A common problem is that the eigenvalues may not exhibit a clear drop, making the dimension hard to determine even for automatic procedures. Driven by these challenges, our

work introduces the transposed Khatri-Rao product framework, which provides sufficient rank for estimating the number of joint clusters and a clear “elbow” exactly at the joint cluster count.

This rest of this paper is organized as follows. Section 2 introduces our model and presents the proposed transposed Khatri-Rao product method. In Section 3, we study the theoretical statistical performance of our proposed method. We evaluate the empirical performance of our method in clustering and estimating the number of joint clusters, and compare it with MASE in Section 4. Section 5 demonstrates the application to FAO food and agricultural trade data, showing the ability of our approach to uncover joint clusters of countries in the global trade network.

2. METHODOLOGY

2.1. KRAFTY Joint Clustering Methodology

Since V is a small integer, for simplicity, we consider the case of $V = 2$. Before launching into a description of the methodology, we closely examine the relationship between individual clustering matrices $Z^{(1)}$, $Z^{(2)}$, their transposed Khatri-Rao product

$$Z^{(1,2)} = Z^{(1)} \circledast Z^{(2)} \in \{0, 1\}^{n \times K_1 K_2} \quad (2)$$

and the true joint clustering matrix $Z \in C_{n,K}$.

As it is easy to see from Section 1.3 and Figure 1, the matrix Z can be obtained from the matrix $Z^{(1,2)}$ by removing its zero columns. The latter can be accomplished by introducing a matrix $H \in \{0, 1\}^{K_1 K_2 \times K}$, where H is formed by the columns of the identity matrix of order $K_1 K_2$ corresponding to the nonzero columns of $Z^{(1,2)}$. Therefore, with some abuse of notations, for $k_1 \in [K_1]$, $k_2 \in [K_2]$ and $k \in [K]$, one has $H((k_1, k_2), :) = 0$ iff $Z^{(1,2)}(:, (k_1, k_2)) = 0$, and each column of matrix H has one element equal to 1. These definitions imply the following relationships

$$Z = Z^{(1,2)} H, \quad Z^{(1,2)} = Z H^\top, \quad H^\top H = I_K, \quad H \in O_{K_1 K_2, K}. \quad (3)$$

Here, K satisfies conditions (1), so that $K \leq K_1 K_2$. In addition, $Z \in C_{n,K}$, so it is a clustering matrix.

Algorithm 1. Joint Clustering with KRAFTY

Input: $\widehat{Z}^{(v)} \in C_{n,K_v}$ or $\widehat{U}^{(v)} \in O_{n,K_v}$, $v = 1, 2$; the final number of clusters K ; parameter $\epsilon > 0$

Output: Estimated joint clustering function $\hat{z} : [n] \rightarrow [K]$

Steps:

1: Obtain matrix \widehat{U} using formula (6) or (8)

2: Cluster n rows of \widehat{U} into K clusters using $(1 + \epsilon)$ -approximate k -means clustering to obtain the estimated clustering function \hat{z} .

If we knew the true matrices $Z^{(1)}$ and $Z^{(2)}$, then matrix Z in (3) would provide the joint clustering assignment. However, we are given either their estimated versions $\widehat{Z}^{(v)} \in C_{n,K_v}$, or estimated matrices of singular vectors $\widehat{U}^{(v)} \in O_{n,K_v}$, $v = 1, 2$, that can be used for finding individual clustering assignments. In order to design a unified clustering procedure, consider diagonal

matrices

$$D^{(1,2)} = \left(Z^{(1,2)} \right)^\top Z^{(1,2)}, \quad D = Z^\top Z, \quad (4)$$

and observe that, due to (3), one has $D = H^\top D^{(1,2)} H$. Here, $D(k, k) = n_k$, the number of elements in the joint cluster $k \in [K]$. Then it follows from (2) and (4) that

$$U = Z D^{-1/2} = Z^{(1,2)} H D^{-1/2} \in \mathcal{O}_{n,K} \implies Z^{(1,2)} = \left(Z^{(1)} \otimes_{\mathbb{K}} Z^{(2)} \right) = U D^{1/2} H^\top, \quad (5)$$

and the second equality gives the SVD of the matrix $Z^{(1,2)}$. Here rows of U are distinct and correspond to K clusters, hence the clustering assignment $z : [n] \rightarrow [K]$ can be obtained by clustering rows of the matrix U . Moreover, U can be obtained as the top K left singular vectors of $Z^{(1,2)}$, i.e., $U = \text{SVD}_K \left(Z^{(1,2)} \right)$. When one has $\widehat{Z}^{(v)}$ instead of $Z^{(v)}$, $v = 1, 2$, the matrix U can be replaced by

$$\widehat{U} = \text{SVD}_K \left(\widehat{Z}^{(1,2)} \right), \quad \widehat{Z}^{(1,2)} = \left(\widehat{Z}^{(1)} \otimes_{\mathbb{K}} \widehat{Z}^{(2)} \right). \quad (6)$$

Now, consider the case where data consist of matrices

$$U^{(v)} = Z^{(v)} \left(D^{(v)} \right)^{-1/2} \in \mathcal{O}_{n,K_v}, \quad D^{(v)} = \left(Z^{(v)} \right)^\top Z^{(v)}, \quad v = 1, 2.$$

Then, due to property **P1** of Khatri-Rao product (see Section A.6) and properties of the Kronecker product, one has

$$U^{(1)} \otimes_{\mathbb{K}} U^{(2)} = \left(Z^{(1)} \left(D^{(1)} \right)^{-1/2} \right) \otimes_{\mathbb{K}} \left(Z^{(2)} \left(D^{(2)} \right)^{-1/2} \right) = Z^{(1,2)} \left(D^{(1)} \otimes D^{(2)} \right)^{-1/2}$$

Hence, it follows from (5) that U and $U^{(1)} \otimes_{\mathbb{K}} U^{(2)}$ are related as

$$U^{(1,2)} := U^{(1)} \otimes_{\mathbb{K}} U^{(2)} = U D^{1/2} H^\top \left(D^{(1)} \otimes D^{(2)} \right)^{-1/2}.$$

The right-hand side of this equation is not an SVD of $U^{(1,2)}$. In order to obtain an SVD of $U^{(1,2)}$ consider a diagonal matrix \widetilde{D} which places $n_{k_1}^{(1)} n_{k_2}^{(2)}$ in the k th diagonal entry when the k th joint cluster corresponds to clusters k_1 and k_2 in the individual views:

$$\widetilde{D} = H^\top \left(D^{(1)} \otimes D^{(2)} \right) H \in \mathbb{R}^{K \times K}.$$

$\widetilde{D} \neq D$ due to $D^{(1,2)} \neq D^{(1)} \otimes D^{(2)}$. We have that $H^\top \left(D^{(1)} \otimes D^{(2)} \right)^{-1/2} = \widetilde{D}^{-1/2} H^\top$, and therefore

$$U^{(1,2)} = \left(U^{(1)} \otimes_{\mathbb{K}} U^{(2)} \right) = U D^{1/2} \widetilde{D}^{-1/2} H^\top. \quad (7)$$

Since the matrix $D^{1/2} \widetilde{D}^{-1/2}$ is diagonal, this equation provides an SVD of $U^{(1,2)}$ with the matrix U of the left singular vectors, i.e., $U = \text{SVD}_K \left(U^{(1,2)} \right)$. Again, if matrices $\widehat{U}^{(v)}$ are available instead of $U^{(v)}$, $v = 1, 2$, the matrix U can be replaced by \widehat{U} where

$$\widehat{U} = \text{SVD}_K \left(\widehat{U}^{(1,2)} \right), \quad \widehat{U}^{(1,2)} = \left(\widehat{U}^{(1)} \otimes_{\mathbb{K}} \widehat{U}^{(2)} \right). \quad (8)$$

A visual comparison of the results of using $\widehat{U}^{(v)}$ or $\widehat{Z}^{(v)}$ as inputs to KRAFTY is provided in Appendix Figure 13.

2.2. Joint Clustering Algorithms

To obtain a joint clustering from the transposed Khatri-Rao matrix, we can simply apply a clustering algorithm to the rows of \tilde{U} obtained via Equation (6) or (8). This is described in Algorithm 1.

As mentioned above, another way of obtaining joint clusters is to concatenate the matrices $\widehat{Z}^{(v)}$ or $\widehat{U}^{(v)}$, $v = 1, 2$. We refer to this method as MASE since it can be viewed as a version of MASE in Arroyo et al. (2020). The steps are provided in Algorithm 2.

Algorithm 2. Joint Clustering with MASE

Input: $\widehat{Z}^{(v)} \in \mathcal{C}_{n, K_v}$ or $\widehat{U}^{(v)} \in \mathcal{O}_{n, K_v}$, $v = 1, 2$; the final number of clusters K ; parameter

$\epsilon > 0$

Output: Estimated joint clustering function $\hat{z} : [n] \rightarrow [K]$

Steps:

1: Construct matrix $\tilde{Z} = [\widehat{Z}^{(1)} | \widehat{Z}^{(2)}]$ or $\tilde{U} = [\widehat{U}^{(1)} | \widehat{U}^{(2)}]$

2: Find $\widehat{U} = \text{SVD}_K(\tilde{Z})$ or $\widehat{U} = \text{SVD}_K(\tilde{U})$

3: Cluster n rows of \widehat{U} into K clusters using $(1 + \epsilon)$ -approximate k -means clustering to obtain the estimated clustering function \hat{z} .

Section 4 will provide a detailed comparison between Algorithms 1 and 2. Here, we shall make just a few remarks. While the matrix Z is a clustering matrix, \tilde{Z} is not. In addition, while $\text{rank}(Z^{(1,2)}) = \text{rank}(U^{(1,2)})$ is equal to the number of clusters, this is not true for $\tilde{Z} = [Z^{(1)} | Z^{(2)}]$ or $\tilde{U} = [U^{(1)} | U^{(2)}]$. The matrices \tilde{Z} and \tilde{U} have ranks at most $K_1 + K_2$, so they can be rank deficient when $K > K_1 + K_2$, as we have shown in Section 1.3.

The clustering algorithm in Algorithms 1 and 2 is suggested to be $(1 + \epsilon)$ -approximate k -means clustering, but this is not the only possible choice. For example, one can use hierarchical clustering or any other appropriate clustering algorithm. In all simulations and real-data analysis in this paper, we use hierarchical clustering, since we found that it produced more stable results under repeated testing than either k -means or Gaussian mixture modeling.

Remark 1. The case of $V \geq 3$. While this section only presents the case of $V = 2$, it is fairly straightforward to extend the KRAFTY methodology to the case of $V \geq 3$. Specifically, for Algorithm 1, $\widehat{Z}^{(1,2)}$ in formula (6) and $\widehat{U}^{(1,2)}$ in (8) should be replaced by, respectively,

$$\widehat{Z}^{(1, \dots, V)} = \left(\widehat{Z}^{(1)} \circledast \dots \circledast \widehat{Z}^{(V)} \right), \quad \widehat{U}^{(1, \dots, V)} = \left(\widehat{U}^{(1)} \circledast \dots \circledast \widehat{U}^{(V)} \right).$$

If one uses Algorithm 2, then in Step 1,

$$\tilde{Z} = \left[\widehat{Z}^{(1)} | \dots | \widehat{Z}^{(V)} \right], \quad \tilde{U} = \left[\widehat{U}^{(1)} | \dots | \widehat{U}^{(V)} \right].$$

Since $\text{rank}(\tilde{Z}) \leq K_1 + \dots + K_V$ is possibly much smaller than K , the latter again will result in rank-deficient clustering.

2.3. A Common Data-Driven Example.

While in the paper we impose no assumptions on the data-generating process, one of the most common settings is the k -means scenario, where the observed data in view v are given by matrix

$$Y^{(v)} = G^{(v)} + \Xi^{(v)} \in \mathbb{R}^{n \times d_v}, \quad v \in [V], \quad (9)$$

where matrix $G^{(v)}$ has K_v distinct rows and $\mathbb{E}(\Xi^{(v)}) = 0$. The latter means that there exist clustering functions $z_v : [n] \rightarrow [K_v]$ such that the i -th row of $G^{(v)}$ is $G^{(v)}(i, :) = \mu_k^{(v)}$, $i \in [n]$, $k \in [K_v]$. If $\mathcal{M}^{(v)} \in \mathbb{R}^{K_v \times d_v}$ with rows $\mu_k^{(v)}$, then in matrix form we have

$$G^{(v)} = Z^{(v)} \mathcal{M}^{(v)}, \quad v = 1, 2. \quad (10)$$

In the above situation, one obtains matrices $\widehat{U}^{(v)} = \text{SVD}_{K_v}(Y^{(v)})$, and possibly clusters \widehat{U} rows of $\widehat{U}^{(v)}$ to obtain matrices $\widehat{Z}^{(v)}$, $v \in [V]$. Matrices $Y^{(v)}$ and $G^{(v)}$ in (9) and (10) can be of any origin. For example, rows $Y^{(v)}(i, :)$ of $Y^{(v)}$ can be independent, with covariance matrices determined by $k = z_v(i)$, so that $\text{Cov}(Y^{(v)}(i, :)) = \Sigma_k^{(v)}$, or they can be adjacency matrices of random graphs.

To further illustrate how the transposed Khatri-Rao product is used in recovering joint clusters, in Figure 2, we show a visual representation of the application of our method to two adjacency matrices generated from the stochastic block models with three underlying clusters. We assume that the joint clustering structure follows Figure 1, so that there are five joint clusters. We first perform the SVD on each of them and extract matrices $\widehat{U}^{(v)}$, $v = 1, 2$. Then, we construct $\widehat{U}^{(1,2)}$ using formula (8) and obtain \widehat{U} as the matrix of left singular vectors of $\widehat{U}^{(1,2)}$. The resulting scree plot of singular values of $\widehat{U}^{(1,2)}$ shows a clear gap after the fifth singular value, indicating $K = 5$ latent joint clusters. Finally, the joint clusters are recovered by applying the k -means algorithm with $K = 5$ to the five left leading singular vectors of the matrix $\widehat{U}^{(1,2)}$.

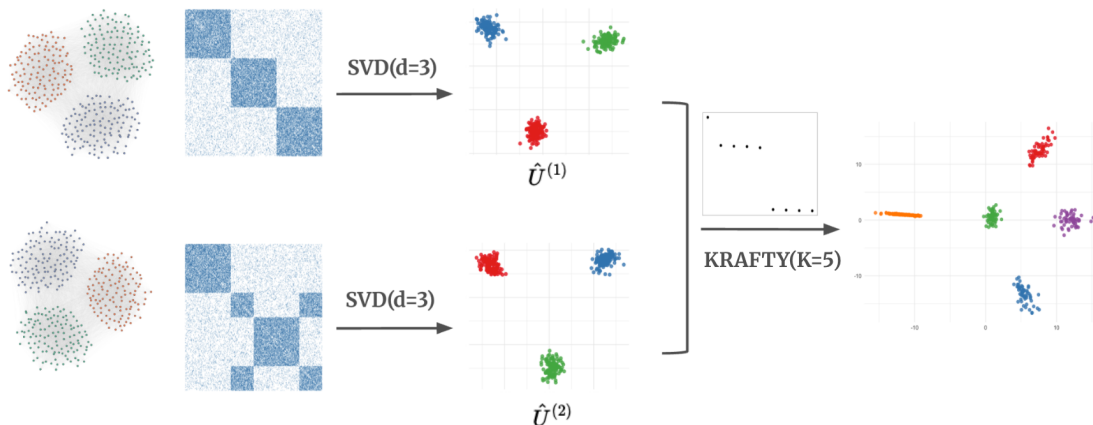


Fig. 2: Graphical representation for a common data-driven example.

3. THEORETICAL RESULTS

3.1. Assumptions

In this section, we present guarantees for joint cluster recovery using KRAFTY (Algorithm 1). As before, for simplicity, we consider the case of $V = 2$, and denote the true clustering matrices by $\widehat{Z}^{(v)}$, $v = 1, 2$. We assume that data come in the form of $\widehat{Z}^{(v)}$ or $\widehat{U}^{(v)}$, $v = 1, 2$. In the former case, let $J_v \subseteq \{1, \dots, n\}$ denote the set of elements misclassified by $\widehat{Z}^{(v)}$ and let $\mathcal{E}_{v,n} = |J_v|$ be its cardinality. Similarly, we denote the true clustering matrix by Z and its estimated version by \widehat{Z} . Let $J \subseteq \{1, \dots, n\}$ denote the set of elements misclassified by \widehat{Z} and let $\mathcal{E}_n = |J|$ be the number of clustering errors.

If data are given in the form of $\widehat{U}^{(v)}$, $v = 1, 2$, we shall place upper bounds on the norms of the differences between $U^{(v)}$ and $\widehat{U}^{(v)}$. Since matrices $\widehat{U}^{(v)}$ are defined only up to a rotation, we consider matrices $W_U^{(v)}$ that deliver the closest match between $U^{(v)}$ and $\widehat{U}^{(v)}$ in Frobenius norm. In particular, if $(U^{(v)})^\top \widehat{U}^{(v)} = W_1 D_W W_2^\top$ is the SVD of $(U^{(v)})^\top \widehat{U}^{(v)}$, then $W_U^{(v)} = W_1 W_2^\top \in \mathcal{O}_{K_v}$.

We say that clustering by \widehat{Z} is *consistent* if $n^{-1} \mathcal{E}_n \rightarrow 0$ as $n \rightarrow \infty$. If $\mathcal{E}_n \rightarrow 0$ as $n \rightarrow \infty$, we say that clustering is *perfect*. In what follows, we show that under straightforward regularity assumptions, clustering precision by Algorithm 1 is as good as individual clusterings, and, in addition, one can correctly identify the number of joint clusters. We begin by stating some regularity assumptions.

Assumption 1 (Balanced cluster sizes). Both the single-view and joint clusterings are assumed to have balanced cluster sizes: if $n_k^{(v)}$ is the number of elements in cluster k in view v , $k \in [K_v]$, and n_k is the number of elements in the joint cluster $k \in [K]$, then for some positive constants, one has

$$\left(c_o^{(v)}\right)^2 \frac{n}{K_v} \leq \min_k n_k^{(v)} \leq \max_k n_k^{(v)} \leq \left(C_o^{(v)}\right)^2 \frac{n}{K_v}, \quad (11)$$

$$c_o^2 \frac{n}{K} \leq \min_k n_k \leq \max_k n_k \leq C_o^2 \frac{n}{K}. \quad (12)$$

Assumption 2 (Finite number of clusters). The number of clusters in each view and, therefore, the number of joint clusters are finite

$$K_1 = O(1), \quad K_2 = O(1), \quad K = O(1), \quad n \rightarrow \infty. \quad (13)$$

Assumption 3 (Consistent clustering in each view). If data are in the form of $\widehat{Z}^{(v)}$, $v = 1, 2$, then the number of clustering errors $\mathcal{E}_{v,n}$ on the basis of $\widehat{Z}^{(v)}$ is such that

$$n^{-1} \mathcal{E}_{v,n} \rightarrow 0, \quad \text{as } n \rightarrow \infty. \quad (14)$$

Assumption 4 (Consistent subspace estimation). If data are in the form of $\widehat{U}^{(v)}$, $v = 1, 2$, then, for some non-random quantities $\mathcal{E}_{0n}^{(v)}$ and $\mathcal{E}_{2,\infty,n}^{(v)}$, $v = 1, 2$ and an arbitrary constant $\tau > 0$, one has

$$\mathbb{P} \left\{ \left\| \widehat{U}^{(v)} - U^{(v)} W_U^{(v)} \right\| \leq C_\tau \mathcal{E}_{0,n}^{(v)} \right\} \geq 1 - n^{-\tau}, \quad (15)$$

$$\mathbb{P} \left\{ \left\| \widehat{U}^{(v)} - U^{(v)} W_U^{(v)} \right\|_{2,\infty} \leq C_\tau \mathcal{E}_{2,\infty,n}^{(v)} \right\} \geq 1 - n^{-\tau}, \quad (16)$$

where the constant C_τ depends on τ only.

Assumption 5 (Incoherence of $\widehat{U}^{(v)}$). For $v = 1$ or $v = 2$ and a constant C_τ that depends on τ only, one has

$$\mathbb{P} \left\{ \left\| \widehat{U}^{(v)} \right\|_{2,\infty} \leq C_\tau \frac{\sqrt{K_v}}{\sqrt{n}} \right\} \geq 1 - n^{-\tau}. \quad (17)$$

The assumptions above are quite common. Assumption 1 allows cluster sizes to vary up to constant factors. If the clusters are highly unbalanced, then it is very hard to distinguish between an erroneous cluster and a genuine very small cluster. Assumption 2 states that we are interested in the setting where the number of clusters in each view is fixed and does not grow with n . Assumption 3 addresses the situation where data come in the form of estimated clustering matrices, such that estimated individual clustering assignments are consistent with high probability. Assumption 4 handles the case where the data appear as estimated matrices of singular vectors. It postulates that,

with high probability, the spectral and the two-to-infinity norms of the differences are bounded above by some non-random quantities. The only condition that appears somewhat unusual is Assumption 5. However, this assumption can be satisfied in a variety of ways. It is easy to see that (17) holds if $\mathcal{E}_{2,\infty,n}^{(v)} \leq C K_v^{1/2} n^{-1/2}$. The latter is true, for example, if one is dealing with the k -means model (9), where the error matrix $\Xi^{(v)}$ has independent sub-gaussian entries. For instance, the following statement follows directly from Theorem 3.1 of Xie & Zhang (2025).

LEMMA 1 (INCOHERENCE OF MATRIX $\widehat{U}^{(v)}$). *Consider model (9) with $G^{(v)}$ given by (10). Let $d_v \geq K_v$ and the ratio between the smallest and the largest nonzero eigenvalues of $\mathcal{M}^{(v)}$ is bounded below by a constant, i.e.*

$$\sigma_{K_v}(G^{(v)}) \Big/ \sigma_1(G^{(v)}) \geq C_\sigma.$$

Suppose the elements of the matrix $\Xi^{(v)}$ in (9) are independent sub-gaussian or sub-exponential random variables, so that, for any $t > 0$ and some absolute constant $C > 0$, one has

$$\mathbb{P} \{ \sigma^{-1} |\Xi(i, j)| > t \} \leq C \exp(-t^a),$$

where $a = 2$ for the sub-gaussian and $a = 1$ for the sub-exponential case. Then, condition (17) in Assumption 5 is satisfied provided

$$\sigma \sqrt{n} (\log n)^{1+\xi} \Big/ \sigma_{K_v}(G^{(v)}) = O(1)$$

for some $\xi > 0$.

Another way to ensure validity of Assumption 5 is to modify Algorithm 1 by adding a regularization step. Define a regularization operator $\mathcal{P}_\delta(U, K)$ as

$$\mathcal{P}_\delta(U) = \text{SVD}_K(U_*) \quad \text{where} \quad U_*(i, :) := U(i, :) \cdot \min \{ \delta, \|U(i, :)\| \} \Big/ \|U(i, :)\|, \quad i \in [n].$$

Before applying Algorithm 1, replace one of the matrices $\widehat{U}^{(v)}$ by $\widehat{U}_\delta^{(v)}$,

$$\widehat{U}_\delta^{(v)} = \mathcal{P}_{\delta_v} \left(\widehat{U}^{(v)}, K_v \right), \quad \delta_v = C_v K_v^{1/2} n^{-1/2}, \quad v = 1, 2,$$

where C_v is a sufficiently large constant. Subsequently, obtain matrix \widehat{U} in Step 1 of Algorithm 1 using formula

$$\widehat{U} = \text{SVD}_K \left(\widehat{U}^{(1,2)} \right), \quad \widehat{U}^{(1,2)} = \left(\widehat{U}_{\delta_1}^{(1)} \mathbb{R} \widehat{U}^{(2)} \right) \quad \text{or} \quad \widehat{U}^{(1,2)} = \left(\widehat{U}^{(1)} \mathbb{R} \widehat{U}_{\delta_2}^{(2)} \right)$$

instead of (8). In this case, $\widehat{U}_{\delta_v}^{(v)}$ will satisfy Assumption 5, and together with Assumption 1, Equation (16) holds for this view with $\mathcal{E}_{2,\infty,n}^{(v)} = n^{-1/2} K_v^{1/2}$. In addition, by properties of regularization (see, e.g., Kim et al. (2018) or Kivelä et al. (2014)), one has

$$\left\| \widehat{U}_{\delta_v}^{(v)} - U^{(v)} W_{U,\delta}^{(v)} \right\| \leq 2\sqrt{2} \left\| \widehat{U}^{(v)} - U^{(v)} W_U^{(v)} \right\|,$$

so Equation (15) holds with the same $\mathcal{E}_{0,n}^{(v)}$ for the regularized version $\widehat{U}_\delta^{(v)}$ of $\widehat{U}^{(v)}$, with a different constant C_τ .

3.2. Accuracy of Joint Cluster Recovery

In this section, we evaluate the precision of Algorithm 1. We assume that the number of clusters K_v , $v = 1, 2$, in each view, and the number of joint clusters K are known. We start with the case when one observes $\widehat{Z}^{(v)}$, $v = 1, 2$.

THEOREM 1 (ACCURACY OF JOINT CLUSTER RECOVERY ON THE BASIS OF $\widehat{Z}^{(v)}$). *Let Assumptions 1,2,3 hold, and suppose that the joint clustering assignment \hat{z} is obtained using Algorithm 1 applied to $\widehat{Z}^{(v)}$, $v = 1, 2$. If n is large enough, the number of clustering errors \mathcal{E}_n for the clustering \hat{z} is at most the sum of clustering errors in the individual views $\widehat{Z}^{(1)}$ and $\widehat{Z}^{(2)}$, i.e.,*

$$\mathcal{E}_n \leq \mathcal{E}_{1,n} + \mathcal{E}_{2,n}. \quad (18)$$

Therefore, if the clusterings $\widehat{Z}^{(v)}$ for $v = 1, 2$ are consistent, then clustering on the basis of \widehat{Z} is consistent. If the clusterings $\widehat{Z}^{(v)}$, $v = 1, 2$, are perfect, then clustering on the basis of \widehat{Z} is also perfect.

Now, consider the case where data come in the form of estimated matrices of singular vectors $\widehat{U}^{(v)}$, $v = 1, 2$.

THEOREM 2 (CONSISTENT RECOVERY OF JOINT CLUSTERS ON THE BASIS OF $\widehat{U}^{(v)}$). *Let Assumptions 1, 2, 4, and 5 hold and $\mathcal{E}_{0,n}^{(v)} = o(1)$ as $n \rightarrow \infty$ for $v = 1, 2$. Then, clustering using Algorithm 1 applied to $\widehat{U}^{(v)}$, $v = 1, 2$ is consistent.*

THEOREM 3 (PERFECT CLUSTERING). *Let the conditions of Theorem 2 hold and, in addition, for $v = 1, 2$*

$$\sqrt{n/K_v} \mathcal{E}_{2,\infty,n}^{(v)} = o(1), \quad \text{as } n \rightarrow \infty. \quad (19)$$

Then for large enough n , clustering using Algorithm 1 applied to $\widehat{U}^{(v)}$, $v = 1, 2$ is perfect with high probability.

If one uses the $\widehat{U}^{(v)}$ -based version of Algorithm 1, the condition $\mathcal{E}_{0,n}^{(v)} = o(1)$ is necessary for consistent clustering in each view v . In order for clustering to be perfect under Assumptions 1, 2, 4, and 5, one needs $\sqrt{n/K_v} \mathcal{E}_{2,\infty,n}^{(v)}$ to be bounded by a small absolute constant, and the theorem remains true under this weaker condition (though the constant is hard to specify).

In our simulations, we found that hierarchical clustering with complete linkage (see Algorithm 3) exhibited more stable performance for joint clustering compared to k -means or Gaussian mixture modeling, so we provide a similar result for the version of Algorithm 1 in which we replace $(1 + \epsilon)$ -approximate k -means with this algorithm.

THEOREM 4 (PERFECT CLUSTERING WITH HC). *Let the conditions of Theorem 3 hold, and let \widehat{U} be the result of Algorithm 1 applied to $\widehat{U}^{(v)}$, $v = 1, 2$. Then when n is large enough, clustering using Algorithm 3 applied to the rows of \widehat{U} yields a perfect clustering at step $t = n - K + 1$ with high probability.*

3.3. Estimating the Number of Joint Clusters

As we have discussed earlier, one of the advantages of the KRAFTY algorithm is that it enables a more accurate estimation of the number of joint clusters, especially when $K > K_1 + K_2$. The following statements confirm that the singular values of matrices $\widehat{Z}^{(1,2)}$ and $\widehat{U}^{(1,2)}$, defined in (6) and (8) respectively, exhibit elbows at the K -th singular values.

Algorithm 3. Complete-Linkage Hierarchical Clustering**Input:** $\widehat{U}(i, :) \in \mathbb{R}^K, i \in [n]$.**Output:** Clustering partitions $\mathcal{G}^{(t)}$ and merge heights $h(t)$ for $t = 1, \dots, n$.**Steps:****1:** Initialize $\mathcal{G}_1^{(0)} = \{\{1\}, \{2\}, \dots, \{n\}\}$;**2: for** $t = 2$ **to** n **do** Find the pair of clusters $(G_i^{(t-1)}, G_j^{(t-1)})$ that minimizes the quantity:

$$d(G_i^{(t-1)}, G_j^{(t-1)}) = \max\{\|\widehat{U}(a, :) - \widehat{U}(b, :)\| : a \in G_i^{(t-1)}, b \in G_j^{(t-1)}\}$$

 Merge $G_i^{(t-1)}$ and $G_j^{(t-1)}$ to form $G_{new}^{(t)} = G_i^{(t-1)} \cup G_j^{(t-1)}$; Set $h(t) = \max\{\|\widehat{U}(a, :) - \widehat{U}(b, :)\| : a, b \in G_{new}^{(t)}\}$; Update $\mathcal{G}^{(t)} = (\mathcal{G}^{(t-1)} \setminus \{G_i^{(t-1)}, G_j^{(t-1)}\}) \cup \{G_{new}^{(t)}\}$;

THEOREM 5 (CONSISTENT ESTIMATION OF THE NUMBER OF JOINT CLUSTERS ON THE BASIS OF $\widehat{Z}^{(v)}$). Let Assumptions 1, 2, and 3 hold, and let $\mathcal{E}_{v,n}$ be as defined in (14). Then

$$\sigma_K(\widehat{Z}^{(1,2)}) - \sigma_{K+1}(\widehat{Z}^{(1,2)}) \geq \frac{c_o \sqrt{n}}{\sqrt{K}} \left(1 - \frac{2\sqrt{2}}{c_o} \sqrt{\frac{K(\mathcal{E}_{1,n} + \mathcal{E}_{2,n})}{n}} \right), \quad (20)$$

$$\sigma_{K+j}(\widehat{Z}^{(1,2)}) - \sigma_{K+j+1}(\widehat{Z}^{(1,2)}) \leq \frac{c_o \sqrt{n}}{\sqrt{K}} \frac{2\sqrt{2}}{c_o} \sqrt{\frac{K(\mathcal{E}_{1,n} + \mathcal{E}_{2,n})}{n}}, \quad j \geq 1. \quad (21)$$

Since $n^{-1}(\mathcal{E}_{1,n} + \mathcal{E}_{2,n}) = o(1)$ as $n \rightarrow \infty$, the singular values display an elbow at K when n is large enough.

THEOREM 6 (CONSISTENT ESTIMATION OF THE NUMBER OF JOINT CLUSTERS ON THE BASIS OF $\widehat{U}^{(v)}$). Let Assumptions 1, 2, 4, and 5 hold and $\mathcal{E}_{o,n}^{(v)}$ in (15) be such that $\mathcal{E}_{o,n}^{(v)} = o(1)$ as $n \rightarrow \infty$, $v = 1, 2$. Then

$$\sigma_K(\widehat{U}^{(1,2)}) - \sigma_{K+1}(\widehat{U}^{(1,2)}) \geq \frac{c_D \sqrt{K}}{\sqrt{K_1 K_2} n} \left[1 - \frac{2C_\tau K_1 K_2}{c_D \sqrt{K}} (\mathcal{E}_{o,n}^{(1)} + \mathcal{E}_{o,n}^{(2)}) \right], \quad (22)$$

$$\sigma_{K+j}(\widehat{U}^{(1,2)}) - \sigma_{K+j+1}(\widehat{U}^{(1,2)}) \leq \frac{c_D \sqrt{K}}{\sqrt{K_1 K_2} n} \left[\frac{2C_\tau K_1 K_2}{c_D \sqrt{K}} (\mathcal{E}_{o,n}^{(1)} + \mathcal{E}_{o,n}^{(2)}) \right], \quad j \geq 1. \quad (23)$$

Since $\mathcal{E}_{o,n}^{(1)} + \mathcal{E}_{o,n}^{(2)} = o(1)$ as $n \rightarrow \infty$, the singular values display an elbow at K when n is large enough.

A similar result holds for the case of hierarchical clustering with complete linkage, if we base our estimate of the number of clusters on an elbow in the merge heights $h(t)$.

THEOREM 7 (CONSISTENT ESTIMATION OF THE NUMBER OF JOINT CLUSTERS WITH HC). Let the conditions of Theorem 4 hold, and consider clustering using Algorithm 3 applied to the rows of $\widehat{U}^{(1,2)}$. When n is large enough, with high probability there is an elbow in the merge heights at step $n - K + 2$, in the following sense: For any fixed $\eta \in (0, 1/6)$, once n is large enough, with

high probability we have

$$h(n - K + 2) - h(n - K + 1) \geq (1 - 4\eta) \frac{\sqrt{2K_1 K_2}}{c_o^{(1)} c_o^{(2)} n},$$

$$h(k + 1) - h(k) \leq 2\eta \frac{\sqrt{2K_1 K_2}}{c_o^{(1)} c_o^{(2)} n}, \quad k \leq n - K.$$

Simulation results demonstrating this phenomenon can be found in Appendix Figure 12.

4. SIMULATION RESULTS

4.1. Simulation Design

In this section, we evaluate the empirical performance of KRAFTY in joint clustering and cluster number estimation through simulations, comparing it with MASE under two input settings: (1) $\widehat{U}^{(v)}$ matrices from SVD on each view, and (2) $\widehat{Z}^{(v)}$ matrices obtained by applying k -means to $\widehat{U}^{(v)}$.

The simulation data are generated from Gaussian mixtures characterized by three parameters: the dimension (p), the within-cluster variance (σ^2), and the number of components (K). To obtain the joint cluster labels, we initialize a $K_1 \times K_2$ probability matrix with a number of nonzeros equal to the true number of joint clusters K . After ensuring that there is at least one point within each joint cluster, the remaining points are drawn according to a Multinomial distribution with the specified probability vector. For each dataset $v \in 1, 2$, we sample K_v distinct cluster centers from a standard multivariate normal distribution $\mathcal{N}(\mathbf{0}, I_p)$. The resulting cluster means are denoted by $\boldsymbol{\mu}_k^{(v)}, k \in [K_v]$.

Observations in each dataset are then generated by

$$\mathbf{Y}_i^{(v)} \sim \mathcal{N}(\boldsymbol{\mu}_{\tau_v(i)}^{(v)}, \sigma^2 I_p), \quad i = 1, \dots, n.$$

To evaluate performance across different conditions, we design three scenarios, each varying one parameter while keeping the others fixed.

After generating the datasets, we prepare the inputs to KRAFTY and MASE. Both methods require two inputs, data matrices and number of joint clusters, which are obtained as follows. For the matrices input, when using $\widehat{U}^{(v)}$ matrices, we perform SVD on each dataset and extract the top K_1 and K_2 left singular vectors to form $\widehat{U}^{(v)}$. These two matrices are used as inputs to KRAFTY or MASE. When using $\widehat{Z}^{(v)}$ matrices, we apply k -means clustering to $\widehat{U}^{(v)}$ with $k = K_1$ or $k = K_2$, and use the resulting $\widehat{Z}^{(v)}$ matrices as inputs. To emphasize the comparison between KRAFTY and MASE, we take the number of clusters within individual datasets, K_1 and K_2 , as known. In applications, these numbers would also need to be estimated, but one can make use of standard methods for doing this Zhu & Ghodsi (2006). For the other input, the number of joint clusters, when K is unknown, we use the automatic scree plot selection method of Zhu & Ghodsi (2006), choosing the second elbow as \widehat{K} since the first one often corresponds to a single dominant dimension rather than the true cluster structure. The automatic scree plot selection method is used for two main reasons: (1) it offers an objective and reproducible criterion for estimating K , and (2) it facilitates fully automated estimation across the large number of experimental replications required in our study. Under known K condition, we use K as the input.

Applying k -means clustering to the individual views to obtain $\widehat{Z}^{(v)}$ provides stable results, but is less consistent for clustering the rows of \widehat{U} after applying KRAFTY or MASE, so we use hierarchical clustering with complete linkage to do the final clustering in all experiments.

For evaluation metrics, we evaluate joint clustering performance using the Adjusted Rand Index (ARI) Hubert & Arabie (1985), which compares the clustering results with the ground truth labels. We evaluate the accuracy of estimation for the joint cluster number using absolute error, defined as the difference between the estimated \widehat{K} and the true K . Results are averaged over 100 repetitions. In all figures, points represent mean values, shaded regions indicate empirical 95% confidence intervals (mean \pm 1.96SE), and KRAFTY is abbreviated as “KR” in the legends.

4.2. Varying Number of Joint Clusters

In this simulation study, we fix the parameters at $p = 20, n = 1000, \sigma^2 = 0.1, K_1 = K_2 = 4$, while varying the true number of joint clusters from 4 to 16, corresponding to the range from $\max(K_1, K_2)$ to $K_1 \times K_2$.

Figure 3 compares the joint clustering performance of KRAFTY and MASE using either $\widehat{U}^{(v)}$ or $\widehat{Z}^{(v)}$ matrices under both known and unknown K conditions. In the left panel, where $\widehat{Z}^{(v)}$ matrices are used as inputs, the three curves overlap and lie above that of MASE under unknown K when $K > K_1 + K_2$, showing that KRAFTY’s advantage in this regime comes from correctly estimating K . In the right panel, where the $\widehat{U}^{(v)}$ matrices are used as inputs, KRAFTY outperforms MASE when $K > K_1 + K_2$ under both known and unknown K conditions.

Figure 4 further compares the joint clustering performance across the four combinations of methods and input types (KRAFTY- $\widehat{Z}^{(v)}$, KRAFTY- $\widehat{U}^{(v)}$, MASE- $\widehat{Z}^{(v)}$, and MASE- $\widehat{U}^{(v)}$) under unknown K setting. The results are shown for three representative values of K (4, 9, and 15), corresponding to cases where K is smaller than, similar to, and greater than $K_1 + K_2$, respectively, and for six noise levels where $\sigma^2 \in \{0.01, 0.05, 0.1, 0.25, 0.5, 1\}$. It shows that across different noise levels and input types, when $K > K_1 + K_2$, KRAFTY exhibits better performance. Moreover, when K is small, KRAFTY with $\widehat{Z}^{(v)}$ matrices performs comparably to MASE with $\widehat{Z}^{(v)}$ and better than the other two combinations, while as K increases, KRAFTY with $\widehat{U}^{(v)}$ matrices achieves better performance.

In Appendix Figures 19 and 20, we compare KRAFTY versus MASE in both the known K and unknown K settings, as well as comparing $\widehat{U}^{(v)}$ versus $\widehat{Z}^{(v)}$ matrices as input to these methods, under various growth rates $K = f(K_1, K_2)$.

Next, we examine the performance of estimating the number of joint clusters for both methods in Figure 5. The heatmap colors represent the difference in mean absolute error between KRAFTY and MASE, with warm colors indicating that KRAFTY performs better and cool colors indicating that MASE performs better. Both panels (using $\widehat{U}^{(v)}$ or $\widehat{Z}^{(v)}$ as inputs) corroborate that KRAFTY outperforms MASE when K is large. It is also worth noting that when using $\widehat{Z}^{(v)}$ matrices (right panel), even for small K , KRAFTY performs comparably to MASE when the noise level is low (here, $\sigma^2 < 0.5$). This finding aligns with our earlier conclusion that when K is small and the noise level is low, KRAFTY with $\widehat{Z}^{(v)}$ matrices is preferable. Appendix Figure 16 further supports this conclusion by directly comparing the use of $\widehat{Z}^{(v)}$ and $\widehat{U}^{(v)}$ matrices. Appendix Figures 21, and 22 extend the analysis to more values of K_1, K_2 , and growth rates $K = f(K_1, K_2)$, providing further evidence in support of our findings.

4.3. Varying Signal-to-Noise Ratios

In this simulation, we study how the dimension and noise level affect the performance of KRAFTY. We fix $K_1 = K_2 = 4$, set $K \in \{6, 12\}$, and vary the noise level $\sigma^2 \in \{0.01, 0.25, 1, 5\}$ and the dimension $p \in \{2, 4, 6, 8, 10, 20, 30, 40, 50\}$. Figure 6 presents the results of joint clustering of KRAFTY and MASE when K is unknown. For both methods, performance improves with increasing dimension up to a certain point and then plateaus. This pattern aligns with intuition: as dimensionality increases, clusters become more separable due to the reduced overlap of noisy

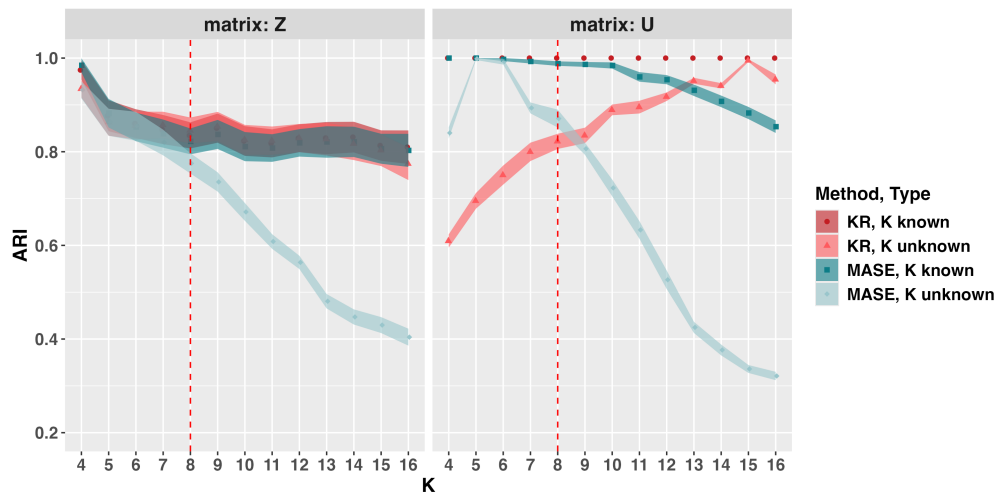


Fig. 3: Joint clustering performance of KRAFTY and MASE using $\widehat{Z}^{(v)}$ or $\widehat{U}^{(v)}$ matrices, evaluated under known and unknown K . ARI measures agreement between estimated and true joint clusters. $K_1 = K_2 = 4$, $\sigma^2 = 0.1$, $p = 20$.

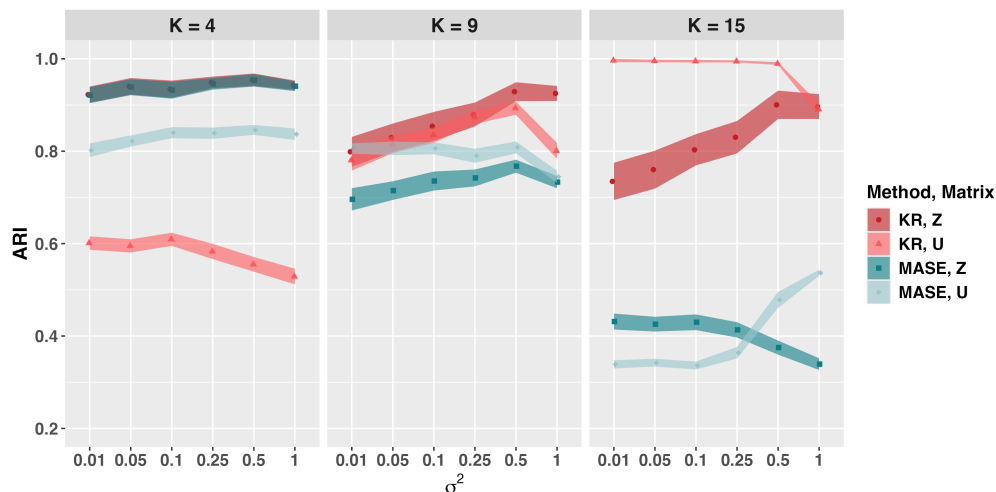


Fig. 4: Joint clustering performance of the $\widehat{Z}^{(v)}$ and $\widehat{U}^{(v)}$ matrices using KR and MASE under **unknown** K setting. The true number of joint clusters K is held constant at 4, 9, and 15 across experiments, with σ^2 varying. ARI compares estimated joint clusters with ground truth. Here, $K_1 = K_2 = 4$, $p = 20$.

data, but once they are sufficiently distinct, further increases in dimension provide little additional benefit.

In the large- K setting, we see that KRAFTY outperforms MASE across several dimensions and noise levels. In the small- K setting, MASE and KRAFTY with $\widehat{Z}^{(v)}$ perform comparably well, with only very low-noise settings showing a preference for MASE with $\widehat{U}^{(v)}$ matrices as input. For low dimensional data, across values of K and noise level, we see that KRAFTY

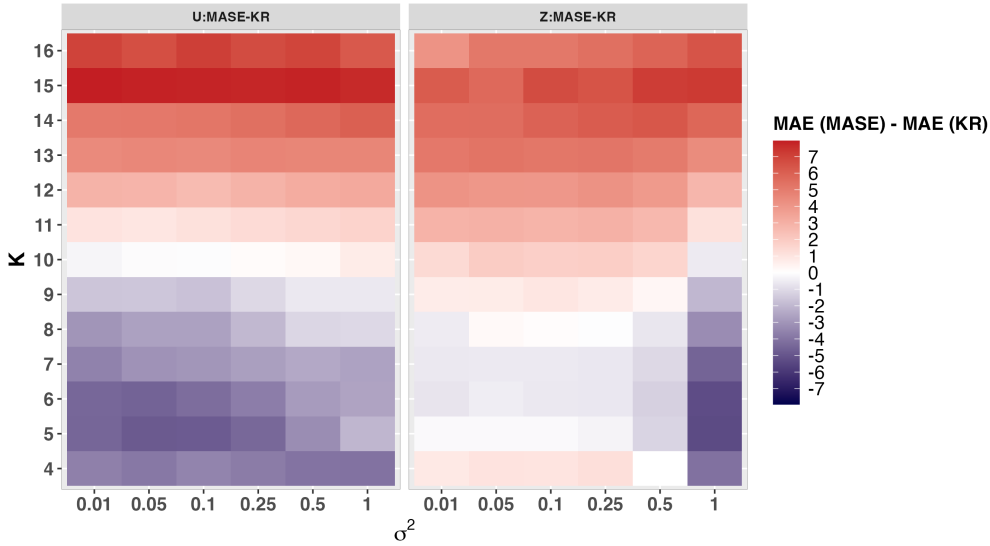


Fig. 5: Comparison of joint cluster number estimation performance between KR and MASE across $\widehat{Z}^{(v)}$ and $\widehat{U}^{(v)}$ matrices, when varying the number of true clusters K and noise level σ^2 . Heatmap colors represent the difference in mean absolute error (averaged over 100 repetitions) when estimating K using MASE versus KR. The width of the largest credible interval for the $\widehat{U}^{(v)}$ matrices ($= 2(1.96)SE$) is 1.06, for the $\widehat{Z}^{(v)}$ matrices it is 1.15. **Cool colors** \rightarrow **MASE better**; **warm colors** \rightarrow **KR better**. $K_1 = K_2 = 4$, $p = 20$.

with $\widehat{Z}^{(v)}$ matrices is an excellent choice, which is perhaps surprising since we expect strong performance from MASE for small values of K . A different view of this comparison can be found in Appendix Figure 17 (fourth panel in the first row), which further corroborates this result, where the warm-colored lower-right triangle indicates KRAFTY's better performance under high-noise conditions, in both low and high K settings.

Comparing $\widehat{Z}^{(v)}$ versus $\widehat{U}^{(v)}$ matrices as inputs, we see that under the same noise and dimension settings, KRAFTY with $\widehat{Z}^{(v)}$ matrices consistently outperforms KRAFTY with $\widehat{U}^{(v)}$ when K is small, while for large K , KRAFTY with $\widehat{U}^{(v)}$ performs better once the signal-to-noise ratio is sufficiently high, as seen in higher dimensions. This pattern is further supported by Figure 7, which directly compares the results of $\widehat{U}^{(v)}$ and $\widehat{Z}^{(v)}$ across all combinations of dimension and noise level. When $K = 6$, the heatmaps are all cool-colored, indicating that KRAFTY with $\widehat{Z}^{(v)}$ performs better. In contrast, when $K = 12$, the upper-left region of the heatmap (corresponding to high dimension relative to noise) is warm-colored, while the lower region is cool-colored, suggesting that KRAFTY with $\widehat{U}^{(v)}$ performs better under high-dimensional, low-noise conditions. A more complete comparison of $\widehat{U}^{(v)}$ versus $\widehat{Z}^{(v)}$ matrices can be found in Appendix Figure 18.

Figure 8 presents the results for estimating the number of joint clusters. The figure is organized such that the left four panels compare $\widehat{U}^{(v)}$ and $\widehat{Z}^{(v)}$ for each method, while the right four panels compare KRAFTY and MASE for each input type. When K is small, MASE performs better, except when using $\widehat{Z}^{(v)}$ under relatively high-dimensional settings, where the difference between KRAFTY and MASE becomes small. In contrast, when K is large, KRAFTY clearly outperforms MASE. Comparing $\widehat{U}^{(v)}$ and $\widehat{Z}^{(v)}$ for KRAFTY, we observe that $\widehat{Z}^{(v)}$ provides more accurate estimates of the number of joint clusters when the dimension is sufficient, while $\widehat{U}^{(v)}$ performs better when the dimension is low and noise level is high. In these settings, $\widehat{Z}^{(v)}$ tends to over-

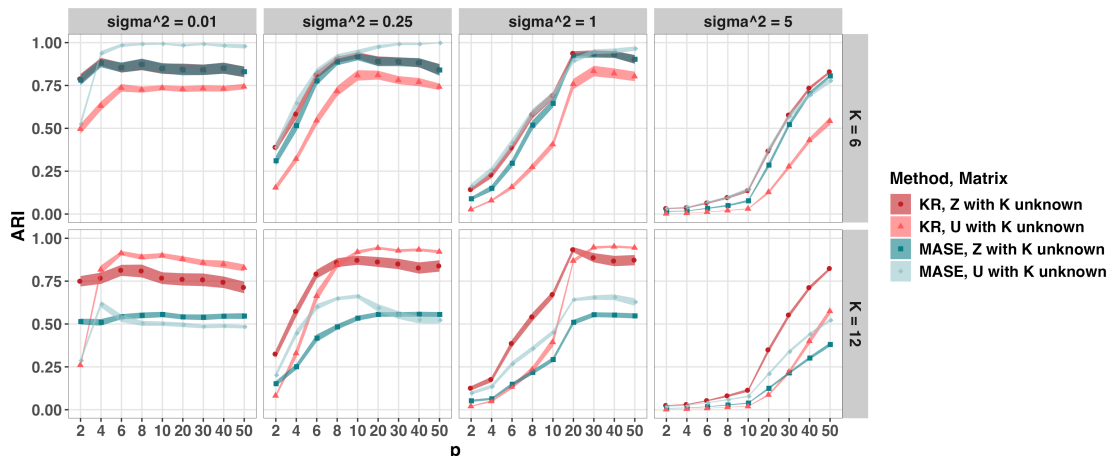


Fig. 6: Comparison of joint clustering performance between KR and MASE across the $\widehat{Z}^{(v)}$ and $\widehat{U}^{(v)}$ matrices when the true number of joint clusters (K) is **unknown**, and the dimension p is varied. ARI is computed by comparing the estimated joint clusters with the ground truth. We set $K_1 = K_2 = 4$, the number of clusters in each single graph.

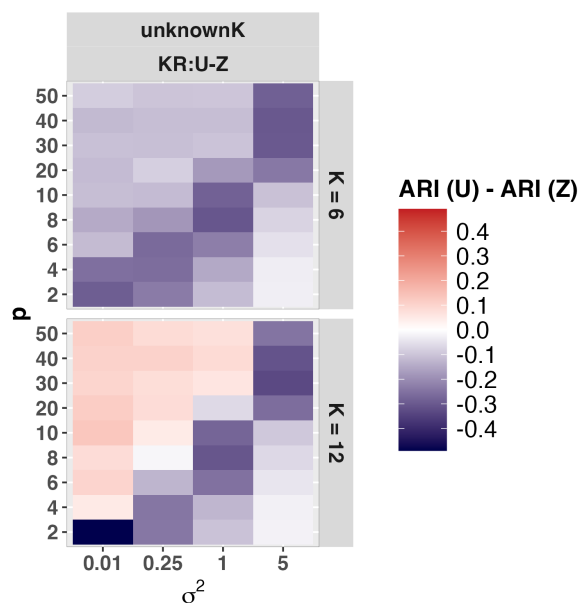


Fig. 7: Comparison of joint clustering performance between $\widehat{Z}^{(v)}$ and $\widehat{U}^{(v)}$ for KRAFTY. Heatmap colors represent the difference in mean ARI (averaged over 100 repetitions) when the number of joint clusters K is **unknown**. **Cool colors** \rightarrow **Z better**; **warm colors** \rightarrow **U better**. $K_1 = K_2 = 4$.

estimate the true number of clusters: this leads to high error on the estimation of the number of joint clusters, but does not lead to a major decrease in clustering performance measured using ARI.

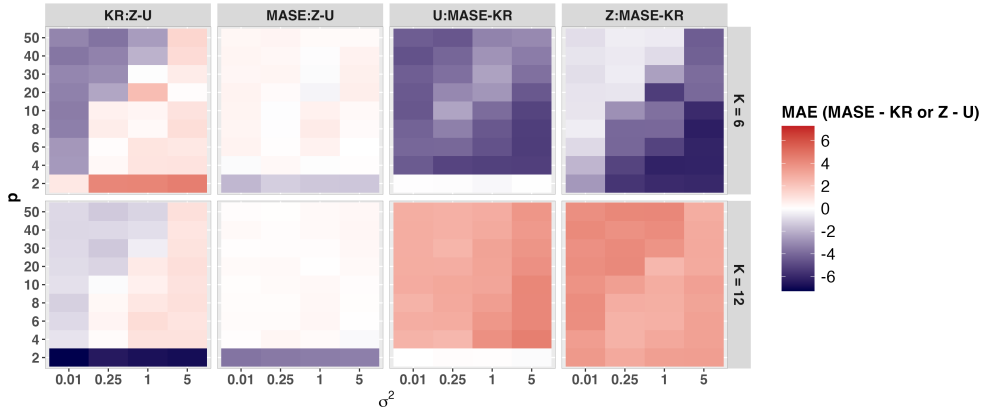


Fig. 8: Comparison of joint cluster number estimation performance between KR and MASE across Z and U matrices, as the dimension p and noise level σ^2 are varied. The left two columns of the heatmap show the difference in mean absolute error (averaged over 100 repetitions) when estimating K using Z versus U. **Cool colors** \rightarrow **Z better**; **warm colors** \rightarrow **U better**. The right 2 columns show the difference in mean absolute error between KR and MASE methods. **Cool colors** \rightarrow **MASE better**; **warm colors** \rightarrow **KR better**. Here, $K_1 = K_2 = 4$.

5. GLOBAL TRADE DATA ANALYSIS

We use the food and agricultural trade dataset provided by the Food and Agriculture Organization (FAO), which is also used in Jing et al. (2021), and is publicly available at <http://www.fao.org>. The data contains a collection of directed, weighted trade networks, one per product, where nodes are countries and edges point from exporters to importers, weighted by the product’s USD trade value.

Following previous work Domenico et al. (2014); Jing et al. (2021); Agterberg & Zhang (2024), we select data from 2010. We also include data from 2023, the most recent available year, in our analysis. The analysis aims (i) to uncover joint clustering structures that capture countries’ joint memberships across their exporting and importing behaviors in 2010, and (ii) to uncover exporter-specific and importer-specific joint clusterings that generalize across years. We focus on one product (raw chicken meat) and analyze two snapshots of its trade network (2010 and 2023), which share an identical vertex set of 191 countries. For each year $v \in \{2010, 2023\}$, let $A^{(v)}$ denote the observed trade matrix (entries are USD exports of the product from row country to column country). We compute its singular value decomposition $A^{(v)} = U^{(v)}\Sigma^{(v)}V^{(v)\top}$, and retain the top three dimensions for 2010 and the top two for 2023, which are selected by Zhu & Ghodsi (2006). Then we estimate countries’ latent positions as exporters and importers by row-normalizing $U^{(v)}(\Sigma^{(v)})^{1/2}$ and $V^{(v)}(\Sigma^{(v)})^{1/2}$ to unit length. The normalized exporter and importer embeddings are denoted $\hat{U}^{(v)}$ and $\hat{V}^{(v)}$, respectively. We then apply k -means with $k = 3$ and $k = 2$ to $\hat{U}^{(v)}$ and $\hat{V}^{(v)}$ to obtain the $\hat{Z}^{(v)} : v \in \{(2010, \text{imp}), (2010, \text{exp}), (2023, \text{imp}), (2023, \text{exp})\}$ matrices as our inputs. We detail the findings for the single-year analysis in this section and leave the double-year analysis to the appendix, since they follow the same analysis procedures.

In this study, we apply both KRAFTY and MASE method to the $\hat{Z}^{(v)} : v \in \{(2010, \text{imp}), (2010, \text{exp})\}$ matrices which are the 2010 importer and exporter cluster assignments, to recover joint groups. Figure 9 shows the scree plots, with a red point marking the estimated number of joint clusters for KRAFTY (Fig. 9(a)) and MASE (Fig. 9(b)). The scree

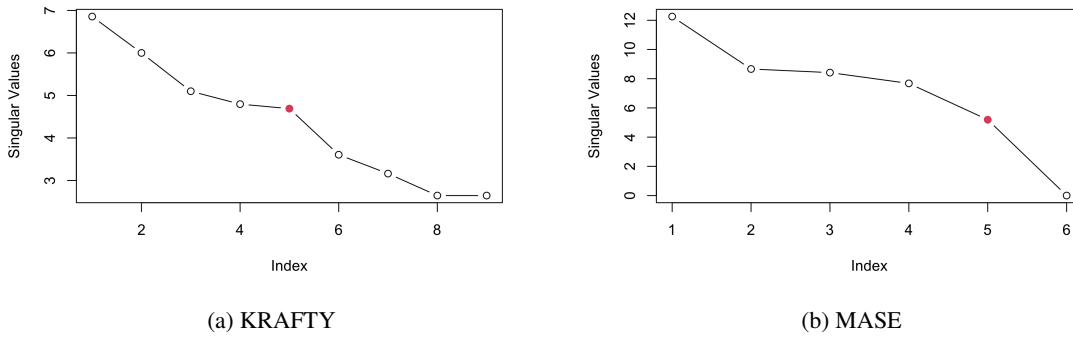


Fig. 9: Eigenvalue scree plot for 2010; the red dot indicates the selected dimension.

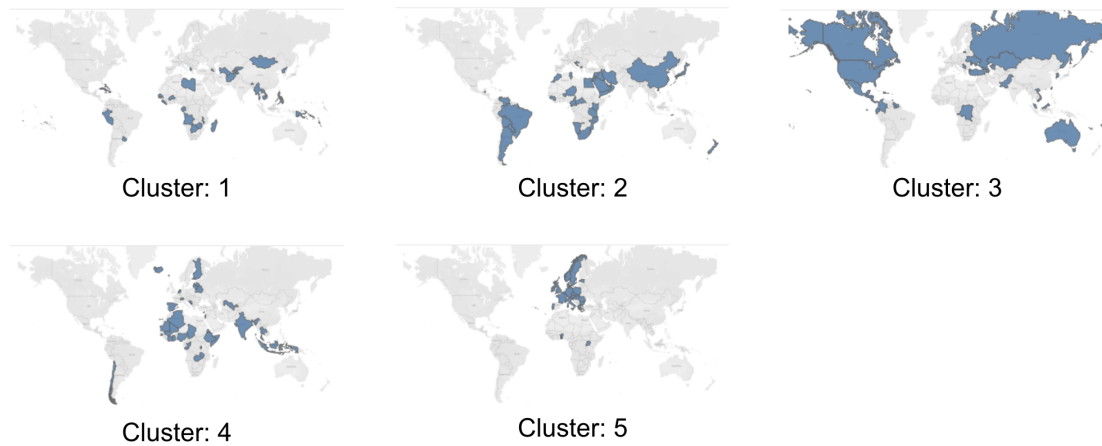


Fig. 10: World map colored by KRAFTY joint clusters for 2010; blue color denotes cluster membership.

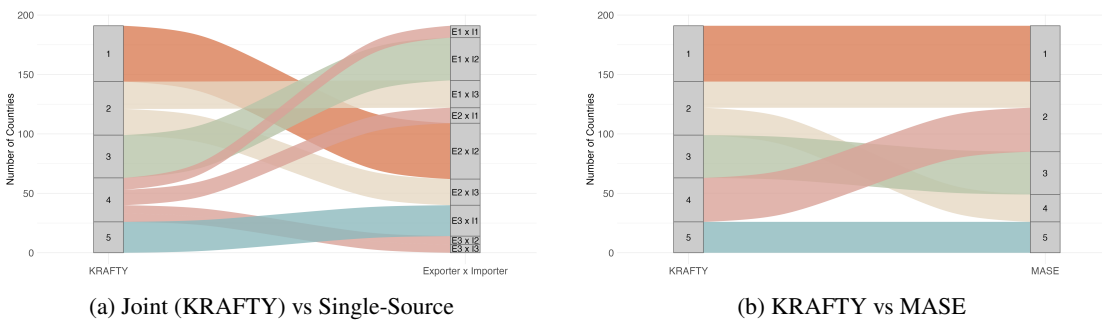


Fig. 11: Alluvial plot comparing cluster assignments for 2010. (a) contrasts KRAFTY’s joint clusters with combinations of single-view clusters; identical colors indicate the same set of entities, and block height reflects the number of countries in each cluster. (b) compares KRAFTY’s joint clusters with those from MASE.

plot of KRAFTY exhibits a distinct elbow, making selection easier, which is consistent with our earlier findings. The appendix scree plots for the two-year exporter and importer analysis also show the same advantage. We use hierarchical clustering in both methods and compare their joint cluster assignments. The ARI is 0.79, which indicates a strong agreement between the two methods. This aligns with our simulations: when the number of joint clusters is smaller than the sum of the single-source clusters, KRAFTY with $\widehat{Z}^{(v)}$ inputs performs similarly to MASE.

Next, we color the world map by joint clusters to see the patterns they reveal; the result is shown in Figure 10. From the colored map, the clusters are primarily regional: Europe, North America, and an Asia–Africa–South America group. This likely reflects the high perishability of raw chicken meat, which favors shorter, regional trading. However, there are exceptions: clusters 1 and 4 appear to mix subsets of Asia–Africa and Europe–Asia–Africa, respectively. These exceptions correspond to groups with significantly lower trading volumes compared to the major regional clusters, as detailed in the trading network heatmap in Appendix Figure 30. Hence, the joint clusters capture both regional patterns and countries’ trading-value behavior. Moreover, we use alluvial plots (Figure 11) to visualize how the joint clusters come from the single-source clusters and to compare where KRAFTY’s joint assignments differ slightly from MASE’s.

6. DISCUSSION

In this work, we propose KRAFTY, a novel joint clustering framework based on the transposed Khatri-Rao product. KRAFTY requires no assumptions about the sources of single-view data and operates directly on either the clustering assignment matrices ($\widehat{Z}^{(v)}$) or low-dimensional spectral embeddings ($\widehat{U}^{(v)}$) from each view. This design makes KRAFTY a flexible and adaptable tool for recovering the joint clustering structure across multiple views. Another appealing feature of KRAFTY is that it supplies sufficient dimension for joint clusters to occupy orthogonal subspaces, unlike concatenation which cannot have rank greater than the sum of the single-view cluster counts. Our main results show that when the number of data points n is large, the joint clustering error is upper-bounded by the sum of the single-view clustering errors. If each single-view clustering is consistent, the joint clustering is also consistent; if the single-view clustering is perfect, the joint clustering is also perfect. This is a desirable property, as researchers can use existing high-quality single-view clustering methods independently and in parallel to achieve accurate joint clustering results. Moreover, we prove that when n is large, the joint embedding produced by KRAFTY has a clear elbow at the true number of joint clusters K , enabling reliable estimation of K using the scree plot or automatic dimension selection methods. In simulations, we systematically compare KRAFTY with the widely used MASE method, as well as evaluate its performance under different input types, $\widehat{Z}^{(v)}$ and $\widehat{U}^{(v)}$. KRAFTY demonstrates strong performance in both clustering assignment accuracy and estimation of the number of joint clusters, particularly when the true number of joint clusters K exceeds the sum of single-view cluster counts. Even when K is smaller than this sum, KRAFTY still achieves comparable performance. In our world trade data analysis, we apply KRAFTY to recover joint clusters of countries based on their roles as exporters and importers.

Finally, we discuss several directions for future work. Although KRAFTY assumes consistent single-view clustering, real-world scenarios often involve noisy, imprecise, or biased clusterings. It would be interesting to explore whether KRAFTY could be used to denoise or refine such noisy inputs through joint structure. Moreover, the presence of evolving cluster structures in many real-world datasets suggests an interesting application of KRAFTY to dynamic community discovery.

7. SUPPLEMENTARY MATERIAL

The Supplementary Material includes proofs for Theorems 1-7, additional simulations, a visual example of KRAFTY, and an additional example on the real data application. The code for simulation and real data analysis is available at GitHub: <https://github.com/Ciel-Gao/KRAFTY>.

REFERENCES

- ABBE, E. (2023). Community detection and stochastic block models.
- ABBE, E., FAN, J. & WANG, K. (2022). An ℓ_p theory of PCA and spectral clustering. *The Annals of Statistics* **50**, 2359–2385.
- AGTERBERG, J., LUBBERTS, Z. & ARROYO, J. (2025). Joint spectral clustering in multilayer degree-corrected stochastic blockmodels.
- AGTERBERG, J. & ZHANG, A. (2024). Estimating higher-order mixed memberships via the $\ell_{2,\infty}$ tensor perturbation bound.
- ARROYO, J., ATHREYA, A., CAPE, J., CHEN, G., PRIEBE, C. E. & VOGELSTEIN, J. T. (2020). Inference for multiple heterogeneous networks with a common invariant subspace.
- DOMENICO, M. D., NICOSIA, V., ARENAS, A. & LATORA, V. (2014). Structural reducibility of multilayer networks. *Nature Communications* **6**.
- FORTUNATO, S. & NEWMAN, M. E. J. (2022). 20 years of network community detection. *Nature Physics* **18**, 848–850.
- GALLAGHER, I., JONES, A. & RUBIN-DELANCHY, P. (2021). Spectral embedding for dynamic networks with stability guarantees. In *Advances in Neural Information Processing Systems*, M. Ranzato, A. Beygelzimer, Y. Dauphin, P. Liang & J. W. Vaughan, eds., vol. 34. Curran Associates, Inc.
- HAN, Q., XU, K. S. & AIROLDI, E. M. (2015). Consistent estimation of dynamic and multi-layer block models.
- HANDCOCK, M. S., RAFTERY, A. E. & TANTRUM, J. M. (2007). Model-based clustering for social networks. *Journal of the Royal Statistical Society Series A: Statistics in Society* **170**, 301–354.
- HOLLAND, P., LASKEY, K. B. & LEINHARDT, S. (1983). Stochastic blockmodels: First steps. *Social Networks* **5**, 109–137.
- HUBERT, L. & ARABIE, P. (1985). Comparing partitions. *Journal of classification* **2**, 193–218.
- JAAGER, A. & BANKS, D. (2023). Cluster analysis: A modern statistical review. *WIREs Computational Statistics* **15**, e1597.
- JIN, D., YU, Z., JIAO, P., PAN, S., HE, D., WU, J., YU, P. S. & ZHANG, W. (2023). A survey of community detection approaches: From statistical modeling to deep learning. *IEEE Transactions on Knowledge and Data Engineering* **35**, 1149–1170.
- JIN, J. (2015). Fast community detection by score. *The Annals of Statistics* **43**.
- JING, B.-Y., LI, T., LYU, Z. & XIA, D. (2021). Community detection on mixture multilayer networks via regularized tensor decomposition. *The Annals of Statistics* **49**, 3181–3205.
- KIM, C., BANDEIRA, A. S. & GOEMANS, M. X. (2018). Stochastic block model for hypergraphs: Statistical limits and a semidefinite programming approach. *arXiv preprint arXiv:1807.02884*.
- KIVELÄ, M., ARENAS, A., BARTHELEMY, M., GLEESON, J. P., MORENO, Y. & PORTER, M. A. (2014). Multilayer networks. *Journal of Complex Networks* **2**, 203–271.
- LEDESMA, R. D., VALERO-MORA, P. & MACBETH, G. (2015). The scree test and the number of factors: a dynamic graphics approach. *The Spanish Journal of Psychology* **18**, E11.
- LEI, J. & LIN, K. Z. (2023). Bias-adjusted spectral clustering in multi-layer stochastic block models. *Journal of the American Statistical Association* **118**, 2433–2445.
- LEI, J. & RINALDO, A. (2015). Consistency of spectral clustering in stochastic block models. *The Annals of Statistics* **43**.
- LYZINSKI, V., SUSSMAN, D., TANG, M., ATHREYA, A. & PRIEBE, C. (2015). Perfect clustering for stochastic blockmodel graphs via adjacency spectral embedding.
- LÖFFLER, M., ZHANG, A. Y. & ZHOU, H. H. (2020). Optimality of spectral clustering in the gaussian mixture model.
- MACDONALD, P. W., LEVINA, E. & ZHU, J. (2021). Latent space models for multiplex networks with shared structure.
- MILLIGAN, G. W. & COOPER, M. C. (1987). Methodology review: Clustering methods. *Applied Psychological Measurement* **11**, 329–354.
- PAUL, S. & CHEN, Y. (2018). Spectral and matrix factorization methods for consistent community detection in multi-layer networks.
- PENSKY, M. (2024). Davis-kahan theorem in the two-to-infinity norm and its application to perfect clustering.
- QIN, T. & ROHE, K. (2013). Regularized spectral clustering under the degree-corrected stochastic blockmodel.
- ROHE, K., CHATTERJEE, S. & YU, B. (2011). Spectral clustering and the high-dimensional stochastic blockmodel. *The Annals of Statistics* **39**.

- SUSSMAN, D. L., TANG, M., FISHKIND, D. E. & PRIEBE, C. E. (2012). A consistent adjacency spectral embedding for stochastic blockmodel graphs.
- TOH, H. & HORIMOTO, K. (2002). Inference of a genetic network by a combined approach of cluster analysis and graphical gaussian modeling. *Bioinformatics* **18**, 287–297.
- VALLÈS-CATALÀ, T., MASSUCCI, F. A., GUIMERÀ, R. & SALES-PARDO, M. (2016). Multilayer stochastic block models reveal the multilayer structure of complex networks. *Phys. Rev. X* **6**, 011036.
- VON LUXBURG, U. (2007). A tutorial on spectral clustering.
- XIE, F. & ZHANG, Y. (2025). Higher-order entrywise eigenvectors analysis of low-rank random matrices: Bias correction, Edgeworth expansion and bootstrap. *The Annals of Statistics* **53**, 1667 – 1696.
- YANG, Y. & WANG, H. (2018). Multi-view clustering: A survey. *Big Data Mining and Analytics* **1**, 83–107.
- ZHU, M. & GHODSI, A. (2006). Automatic dimensionality selection from the scree plot via the use of profile likelihood. *Computational Statistics & Data Analysis* **51**, 918–930.

A. PROOFS OF THE STATEMENTS IN THE PAPER.

A.1. Proof of Theorem 1.

For simplicity, denote

$$X = Z^{(1)} \circledast Z^{(2)} = ZH^\top, \quad \widehat{X} = \widehat{Z}^{(1)} \circledast \widehat{Z}^{(2)}, \quad \Xi = \widehat{X} - X, \quad (\text{A1})$$

where matrix H is defined in (3). Let

$$X = UDH^\top, \quad \widehat{X} = \widehat{U} \widehat{D} \widehat{V}^\top + \widehat{U}^\perp \widehat{D}^\perp (\widehat{V}^\perp)^\top \quad (\text{A2})$$

be the SVDs of X and \widehat{X} . Here, $D = \text{diag}(\sqrt{n_1}, \dots, \sqrt{n_K})$.

Recall that J_v is the set of elements mis-clustered by $\widehat{Z}^{(v)}$ and $\mathcal{E}_{v,n}$, is their number, $v = 1, 2$. Then J_v^c is the set of correctly clustered elements. Denote, $J = J_1 \cup J_2$, $J^c = J_1^c \cap J_2^c$ and observe that, if $i \in J^c$, then $\Xi(i, :) = 0$. Here, due to $|J_v^c| = n - \mathcal{E}_{v,n}$, one has $|J^c| \geq n - (\mathcal{E}_{1,n} + \mathcal{E}_{2,n})$. In order to evaluate the clustering accuracy of Algorithm 1, observe that, by Assumption 1

$$\sigma_K(X) = \min_{k \in [K]} \sqrt{n_k} \geq \frac{c_o \sqrt{n}}{\sqrt{K}}. \quad (\text{A3})$$

Since $\|\widehat{X}(i, :) - X(i, :)\|^2 = 0$ if $i \in J^c$, and $\|\widehat{X}(i, :) - X(i, :)\|^2 = 2$ if $i \in J$, we have

$$\|\widehat{X} - X\|_F^2 = 2|J| \leq 2(\mathcal{E}_{1,n} + \mathcal{E}_{2,n}). \quad (\text{A4})$$

Therefore, $\|\Xi\| = \|\widehat{X} - X\| \leq \sqrt{2(\mathcal{E}_{1,n} + \mathcal{E}_{2,n})}$. Consistency of the individual clusterings (Assumption 3) implies that $n^{-1}\mathcal{E}_{v,n} \rightarrow 0$. Then, for n large enough, one has

$$\sigma_K(\widehat{X}) \geq \sigma_K(X) - \|\widehat{X} - X\| \geq \frac{c_o \sqrt{n}}{\sqrt{K}} \left(1 - \frac{\sqrt{2K}}{c_o} \frac{\sqrt{\mathcal{E}_{1,n} + \mathcal{E}_{2,n}}}{\sqrt{n}} \right) \geq \frac{c_o \sqrt{n}}{2\sqrt{K}}. \quad (\text{A5})$$

Observe that, by Assumption 3, as $n \rightarrow \infty$,

$$\epsilon_{o,n} := \frac{\sqrt{\mathcal{E}_{1,n} + \mathcal{E}_{2,n}}}{\sqrt{n}} = o(1). \quad (\text{A6})$$

Then, by Wedin theorem and Assumptions 2 and 3, as $n \rightarrow \infty$,

$$\max \left(\|\widehat{U} - U W_U\|_F^2, \|\widehat{V} - H W_V\|_F^2 \right) \leq \frac{2 \|\Xi\|_F^2}{\sigma_K^2(X)} \leq \frac{4K(\mathcal{E}_{1,n} + \mathcal{E}_{2,n})}{c_o^2 n} \asymp \epsilon_{o,n}^2 = o(1). \quad (\text{A7})$$

Here, W_U and W_V are the rotations which provides the closest match between \widehat{U} and U , and \widehat{V} and HW_V , respectively. Specifically, if $U^\top \widehat{U} = W_1 D_W W_2^\top$ is the SVD of $U^\top \widehat{U}$, then $W_U = W_1 W_2^\top$.

In order to assess the number of clustering errors on the basis of \widehat{X} , we apply Lemma D1 of Abbe et al. (2022)), which we provide here for readers' convenience.

LEMMA A1. (Lemma D1 of Abbe et al. (2022)). *Let matrix $B \in \mathbb{R}^{r \times m}$ with rows $B(k, :)$, $k \in [K]$, be the matrix of true means and $z : [n] \rightarrow [K]$ be the true clustering function. For a data matrix $\widehat{X} \in \mathbb{R}^{n \times m}$, any matrix $\widetilde{B} \in \mathbb{R}^{K \times m}$ and any clustering function $\tilde{z} : [n] \rightarrow [K]$, define*

$$L(\widetilde{B}, \tilde{z}) = \sum_{i=1}^n \left\| \widehat{X}(i, :) - \widetilde{B}(\tilde{z}(i), :) \right\|^2. \quad (\text{A8})$$

Let $\widehat{B} \in \mathbb{R}^{K \times m}$ and $\hat{z} : [n] \rightarrow [K]$ be solutions to the $(1 + \epsilon)$ -approximate k -means problem, i.e.

$$L(\widehat{B}, \hat{z}) \leq (1 + \epsilon) \min_{\widetilde{B}, \tilde{z}} L(\widetilde{B}, \tilde{z}).$$

Let $s = \min_{i \neq j} \|B(i, :) - B(j, :)\|$ and n_{\min} be the minimum cluster size. If for some $\delta \in (0, s/2)$ one has

$$L(B, z) = \sum_{i=1}^n \left\| \widehat{X}(i, :) - B(z(i), :) \right\|^2 \leq \frac{\delta^2 n_{\min}}{K(1 + \sqrt{1 + \epsilon})^2}, \quad (\text{A9})$$

then there exists a permutation $\phi : [K] \rightarrow [K]$ such that

$$\{i : \hat{z}(i) \neq \phi(z(i))\} \subseteq \left\{i : \|\widehat{X}(i, :) - B(z(i), :)\| \geq s/2 - \delta\right\}, \quad (\text{A10})$$

$$\#\{i : \hat{z}(i) \neq \phi(z(i))\} \leq (s/2 - \delta)^{-2} L(B, z). \quad (\text{A11})$$

We apply Lemma A1 with $s = \min_{i \neq j} \|U(i, :) - U(j, :)\| \geq (2/\max(n_k))^{1/2}$, $X = U W_U$, $B(z(i), :) = X(i, :)$

and $L(B, z) \leq \left\| \widehat{U} - U W_U \right\|_F^2$. Therefore,

$$\delta^2 \leq \frac{\|\widehat{U} - U W_U\|_F^2 K(1 + \sqrt{1 + \epsilon})^2}{\min(n_k)},$$

so that, by (A7), we obtain

$$\frac{s}{2} \geq \frac{\sqrt{K}}{C_o \sqrt{2n}}, \quad \delta \leq \frac{2K(1 + \sqrt{1 + \epsilon})}{c_o^{3/2}} \frac{\sqrt{\mathcal{E}_{1,n} + \mathcal{E}_{2,n}} \sqrt{K}}{n}. \quad (\text{A12})$$

By Lemma A1, row i is clustered correctly, if $\|e_i^\top (\widehat{U} - U W_U)\| < s/2 - \delta$, where

$$\frac{s}{2} - \delta \geq \frac{\sqrt{K}}{C_o \sqrt{2n}} \left(1 - \frac{2\sqrt{2} C_o K(1 + \sqrt{1 + \epsilon})}{c_o^{3/2}} \frac{\sqrt{\mathcal{E}_{1,n} + \mathcal{E}_{2,n}}}{\sqrt{n}} \right),$$

and the second term in the parenthesis is $o(1)$ as $n \rightarrow \infty$ due to Assumption 3. Hence, correct clustering of row i is guaranteed by

$$\|e_i^\top (\widehat{U} - U W_U)\| = o\left(\sqrt{K}/\sqrt{n}\right). \quad (\text{A13})$$

Now, we consider rows with $i \in J^c$ and show that all these rows are clustered correctly. For $i \in J^c$, $e_i^\top \Xi = \Xi(i, :) = 0$.

From (A1) derive that

$$R_i := \|e_i^\top (\widehat{U} - U W_U)\| \leq R_{i1} + R_{i2} + R_{i3} + R_{i4} + R_{i5} \quad (\text{A14})$$

with $\Xi = \widehat{X} - X$ and

$$\begin{aligned} R_{i1} &= \|e_i \Xi H W_V \widehat{D}^{-1}\| = 0, & R_{i2} &= \|e_i^\top \Xi (\widehat{V} - H W_V) \widehat{D}^{-1}\| = 0, \\ R_{i3} &= \|e_i^\top U U^\top \Xi H W_V \widehat{D}^{-1}\|, & R_{i4} &= \|e_i^\top U U^\top \Xi (\widehat{V} - H W_V) \widehat{D}^{-1}\|, \\ R_{i5} &= \|e_i^\top U (U^\top \widehat{U} - W_U)\|. \end{aligned} \quad (\text{A15})$$

Observe that, for n large enough, by (A5), one has

$$\|\widehat{D}^{-1}\| = \sigma_{\min}^{-1}(\widehat{X}) \leq C \sqrt{\frac{K}{n}}.$$

Therefore, using (A4), (A6) and (A7), as $n \rightarrow \infty$, obtain

$$R_{i3} \leq \|U\|_{2,\infty} \|\Xi\| \|\widehat{D}^{-1}\| \leq C(K/\sqrt{n}) \epsilon_{o,n} = o(\sqrt{K}/\sqrt{n}), \quad (\text{A16})$$

$$R_{i4} \leq \|U\|_{2,\infty} \|\Xi\| \|\widehat{D}^{-1}\| \|\widehat{V} - H W_V\| \leq C(K/\sqrt{n}) \epsilon_{o,n}^2 = o(\sqrt{K}/\sqrt{n}), \quad (\text{A17})$$

$$R_{i5} \leq \|e_i^\top U (U^\top \widehat{U} - W_U)\| \leq C(\sqrt{K}/\sqrt{n}) \epsilon_{o,n}^2 = o(\sqrt{K}/\sqrt{n}). \quad (\text{A18})$$

Combination of (A14)–(A18) implies validity of (A13) and, therefore, guarantees that, for n large enough, all elements in J^c are clustered correctly. Then (18) is true and Theorem 1 holds.

A.2. Proof of Theorems 2 and 3.

Without loss of generality, we suppose that Assumption 5 holds with $\nu = 2$. In order to assess the number of clustering errors on the basis of \widehat{U} , we apply Lemma A1 with $s = \min_{z(i) \neq z(j)} \|U(i, :) - U(j, :)\|$,

$X = U W_U$, $B(z(i), :) = X(i, :)$ and $L(B, z) \leq \left\| \widehat{U} - U W_U \right\|_F^2$. Therefore,

$$s \geq \frac{\sqrt{2}}{\sqrt{\max(n_k)}} \geq \frac{\sqrt{2K}}{C_o \sqrt{n}}, \quad \delta \leq \frac{\|\widehat{U} - U W_U\|_F \times \sqrt{K} (1 + \sqrt{1 + \epsilon})}{\sqrt{\min(n_k)}}. \quad (\text{A19})$$

Recall that $U = \text{SVD}_K(U^{(1,2)})$ and $\widehat{U} = \text{SVD}_K(\widehat{U}^{(1)} \otimes \widehat{U}^{(2)})$, where $U^{(1,2)} = U^{(1)} \otimes U^{(2)}$ and $\widehat{U}^{(1,2)} = \widehat{U}^{(1)} \otimes \widehat{U}^{(2)}$. Recall also that, by (7),

$$U^{(1,2)} = U D V^\top, \quad V \equiv H, \quad D = (D_Z \widetilde{D}_Z^{-1})^{1/2}. \quad (\text{A20})$$

Here, $D_Z = Z^\top Z$, so that, for $k_1 \in [K_1]$, $k_2 \in [K_2]$, using double-index, one can write

$$D_Z(k, k) = n_k, \quad \widetilde{D}_Z(k, k) = n_{k_1}^{(1)} n_{k_2}^{(2)} I(H((k_1, k_2), k) = 1), \quad k \in [K].$$

Therefore,

$$D(k, k) = \frac{\sqrt{n_k}}{\sqrt{n_{k_1}^{(1)} n_{k_2}^{(2)}}} I(H((k_1, k_2), k) = 1). \quad (\text{A21})$$

By Assumption 1,

$$\frac{c_D \sqrt{K}}{\sqrt{K_1 K_2} \sqrt{n}} \leq D(k, k) \leq \frac{C_D \sqrt{K}}{\sqrt{K_1 K_2} \sqrt{n}}, \quad (\text{A22})$$

where $c_D = c_o / (C_o^{(1)} C_o^{(2)})$ and $C_D = C_o / (c_o^{(1)} c_o^{(2)})$. The latter, together with (A20) yields

$$\sigma_{\min}(U^{(1,2)}) \geq \frac{c_D \sqrt{K}}{\sqrt{K_1 K_2} \sqrt{n}}. \quad (\text{A23})$$

Write the SVD of $\widehat{U}^{(1,2)}$ as

$$\widehat{U}^{(1,2)} = \widehat{U} \widehat{D} \widehat{V}^\top + \widehat{U}^\perp \widehat{D}^\perp (\widehat{V}^\perp)^\top.$$

Denote $\Xi^{(v)} = \widehat{U}^{(v)} - U^{(v)} W_U^{(v)}$, $v = 1, 2$, and $\Xi = \widehat{U}^{(1,2)} - U^{(1,2)} W_U^{(1,2)}$, where $W_U^{(v)}$ provide the closest matches in the Frobenius norm, and $W_U^{(1,2)} = W_U^{(1)} \otimes W_U^{(2)}$. Let W_V be a rotation matrix which provides the closest match in the Frobenius norm between \widehat{V} and $V W_V$.

Recall that, by Assumptions 2 and 4, as $n \rightarrow \infty$, one has

$$\left\| \Xi^{(v)} \right\|_F = \left\| \widehat{U}^{(v)} - U^{(v)} W_U^{(v)} \right\|_F \leq C_\tau \sqrt{K_v} \mathcal{E}_{0,n}^{(v)} = o(1), \quad v = 1, 2. \quad (\text{A24})$$

Hence,

$$\Xi = \Xi^{(1)} \otimes \widehat{U}^{(2)} + (U^{(1)} W_U^{(1)}) \otimes \Xi^{(2)} \quad (\text{A25})$$

and, by property **P2** of the Khatri-Rao product one has

$$\|\Xi\|_F \leq \|\Xi^{(1)}\|_F \|\widehat{U}^{(2)}\|_{2,\infty} + \|\Xi^{(2)}\|_F \|U^{(1)}\|_{2,\infty}$$

Then Assumptions 1 and 5 and (A24) yield that, with probability at least $1 - 3n^{-\tau}$,

$$\|\Xi\|_F \leq \frac{\tilde{C}_\tau \sqrt{K_1} \sqrt{K_2}}{\sqrt{n}} (\mathcal{E}_{0,n}^{(1)} + \mathcal{E}_{0,n}^{(2)}), \quad (\text{A26})$$

where \tilde{C}_τ is a generic absolute constant that depends on τ and constants in Assumption 1. It is easy to see that the second inequality in (A19) and (A26) immediately yield

$$\delta \leq \frac{\tilde{C}_\tau (1 + \sqrt{1 + \epsilon}) K \sqrt{K_1} K_2 (\mathcal{E}_{0,n}^{(1)} + \mathcal{E}_{0,n}^{(2)})}{c_o n} \quad (\text{A27})$$

Applying the first inequality in (A19), we find that

$$\frac{s}{2} - \delta \geq \frac{\sqrt{K}}{C_o \sqrt{2n}} \left(1 - \frac{\tilde{C}_\tau C_o (1 + \sqrt{1 + \epsilon}) \sqrt{2K} K_1 K_2 (\mathcal{E}_{0,n}^{(1)} + \mathcal{E}_{0,n}^{(2)})}{c_o \sqrt{n}} \right). \quad (\text{A28})$$

If n is large enough, by the conditions of the theorem, one has

$$\frac{s}{2} - \delta \geq \frac{\sqrt{K}}{2\sqrt{2} C_o \sqrt{n}}.$$

Hence, by Lemma A1, row i is guaranteed to be clustered correctly if

$$\|e_i^\top (\hat{U} - UW_U)\| < \frac{\sqrt{K}}{2\sqrt{2} C_o \sqrt{n}}. \quad (\text{A29})$$

In order to utilize (A29), we derive an upper bound for $\|e_i^\top (\hat{U} - UW_U)\|$. We expand the quantity $\Xi V W_V \hat{D}^{-1}$ as

$$\begin{aligned} \Xi V W_V \hat{D}^{-1} &= U U^\top \Xi V W_V \hat{D}^{-1} - (I - U U^\top) \Xi (\hat{V} - V W_V) \hat{D}^{-1} + (I - U U^\top) \Xi \hat{V} \hat{D}^{-1} \\ &= U U^\top \Xi V W_V \hat{D}^{-1} - (I - U U^\top) \Xi (\hat{V} - V W_V) \hat{D}^{-1} + (I - U U^\top) (\hat{U} - UW_U), \end{aligned}$$

making use of the fact that $(I - U U^\top) U^{(1,2)} = 0$, and $\hat{U}^{(1,2)} \hat{V} \hat{D}^{-1} = \hat{U}$. Then for any $i \in [n]$, one has

$$R_i = \|e_i^\top (\hat{U} - UW_U)\| \leq R_{i1} + R_{i2} + R_{i3} + R_{i4} + R_{i5}, \quad i \in [n]. \quad (\text{A30})$$

where

$$\begin{aligned} R_{i1} &= \|e_i^\top \Xi V W_V \hat{D}^{-1}\|, & R_{i2} &= \|e_i^\top \Xi (\hat{V} - V W_V) \hat{D}^{-1}\|, \\ R_{i3} &= \|e_i^\top U U^\top \Xi V W_V \hat{D}^{-1}\|, & R_{i4} &= \|e_i^\top U U^\top \Xi (\hat{V} - V W_V) \hat{D}^{-1}\|, \\ R_{i5} &= \|e_i^\top U (U^\top \hat{U} - W_U)\|. \end{aligned}$$

Observe that, by (A22),

$$\min_k (\hat{D}(k, k)) \geq \min_k (D(k, k)) - \|\Xi\| \geq \frac{c_D \sqrt{K}}{\sqrt{K_1} K_2 \sqrt{n}} \left(1 - \frac{\tilde{C}_\tau K_1 K_2 (\mathcal{E}_{0,n}^{(1)} + \mathcal{E}_{0,n}^{(2)})}{c_D \sqrt{K}} \right). \quad (\text{A31})$$

Therefore, if n is large enough, with high probability,

$$\min_k (\hat{D}(k, k)) \geq \frac{c_D \sqrt{K}}{2 \sqrt{K_1} K_2 \sqrt{n}}, \quad (\text{A32})$$

and we have a similar upper bound with high probability

$$\max_k (\hat{D}(k, k)) \leq \frac{2 C_D \sqrt{K}}{\sqrt{K_1} K_2 \sqrt{n}}. \quad (\text{A33})$$

Since $e_i^\top \Xi = \Xi(i, :)$, (A32) and (A33) lead to

$$R_{i1} = \|e_i^\top \Xi V W_V \widehat{D}^{-1}\| \leq \|\Xi(i, :)\| \frac{2\sqrt{K_1 K_2} \sqrt{n}}{c_D \sqrt{K}}. \quad (\text{A34})$$

By the Davis-Kahan theorem and (A23), we find

$$\|\widehat{V} - V W_V\|_F \leq \frac{C \|\Xi\|_F}{\sigma_{\min}(U^{(1,2)})} \leq \widetilde{C}_\tau \frac{K_1 K_2}{\sqrt{K}} (\mathcal{E}_{0,n}^{(1)} + \mathcal{E}_{0,n}^{(2)}). \quad (\text{A35})$$

Hence, by (A34), with high probability, as $n \rightarrow \infty$,

$$R_{i2} \leq \frac{2\widetilde{C}_\tau}{c_D} \|\Xi(i, :)\| \frac{(K_1 K_2)^{3/2} \sqrt{n}}{K} (\mathcal{E}_{0,n}^{(1)} + \mathcal{E}_{0,n}^{(2)}) = o\left(\|\Xi(i, :)\| \frac{\sqrt{K_1 K_2} \sqrt{n}}{\sqrt{K}}\right). \quad (\text{A36})$$

Now, Assumption 1 and (A32) yield with high probability, if n is large enough,

$$R_{i3} \leq \|U\|_{2,\infty} \|\Xi\| \|\widehat{D}^{-1}\| \leq 2(c_D c_o)^{-1} \sqrt{K_1 K_2} \|\Xi\|.$$

Plugging in $\|\Xi\|_F$ from (A26), we obtain

$$R_{i3} \leq \frac{2\widetilde{C}_\tau K_1 K_2}{c_D c_o \sqrt{n}} (\mathcal{E}_{0,n}^{(1)} + \mathcal{E}_{0,n}^{(2)}). \quad (\text{A37})$$

Similarly, with high probability, as $n \rightarrow \infty$,

$$R_{i4} \leq \|U\|_{2,\infty} \|\Xi\| \|\widehat{D}^{-1}\| \|\widehat{V} - V W_V\| = o(\|U\|_{2,\infty} \|\Xi\| \|\widehat{D}^{-1}\|), \quad (\text{A38})$$

which is upper-bounded in (A37). Finally,

$$R_{i5} \leq C \|U\|_{2,\infty} \|\widehat{U} - U W_U\|^2. \quad (\text{A39})$$

The bound in Equation (A35) applies to $\widehat{U} - U W_U$ as well, so we have

$$R_{i5} \leq C \frac{\sqrt{K}}{c_o \sqrt{n}} \widetilde{C}_\tau^2 \frac{(K_1 K_2)^2}{K} (\mathcal{E}_{0,n}^{(1)} + \mathcal{E}_{1,n}^{(2)})^2 \quad (\text{A40})$$

Since $\mathcal{E}_{0,n}^{(v)} = o(1)$ by assumption of the theorem, this upper bound is much smaller than that of Equation (A37). Hence, for n large enough and $i \in [n]$, combination of (A30)–(A40) yields

$$\|e_i^\top (\widehat{U} - U W_U)\| \leq C_\tau \left(\|\Xi(i, :)\| \frac{\sqrt{K_1 K_2} \sqrt{n}}{\sqrt{K}} + \frac{\sqrt{K_1 K_2}}{\sqrt{n}} (\mathcal{E}_{0,n}^{(1)} + \mathcal{E}_{1,n}^{(2)}) \right), \quad (\text{A41})$$

where the second term in (A41) is asymptotically smaller than \sqrt{K}/\sqrt{n} .

Therefore, validity of inequality (A29) relies entirely on the behavior of $\|\Xi(i, :)\|$. Observe that, by (A25), one has

$$\Xi(i, :) = \left(U^{(1)}(i, :) W_U^{(1)} \right) \circledast \Xi^{(2)}(i, :) + \Xi^{(1)}(i, :) \circledast \widehat{U}^{(2)}(i, :).$$

Hence, due to Assumptions 1 and 5,

$$\|\Xi(i, :)\| \leq \frac{C_\tau \sqrt{K_2}}{\sqrt{n}} \|\Xi^{(1)}(i, :)\| + \frac{\sqrt{K_1}}{c_o^{(1)} \sqrt{n}} \|\Xi^{(2)}(i, :)\|. \quad (\text{A42})$$

Then with high probability for large n ,

$$\|\Xi(i, :)\| \leq C_\tau \left(\frac{C_\tau \sqrt{K_2}}{\sqrt{n}} \mathcal{E}_{2,\infty,n}^{(1)} + \frac{\sqrt{K_1}}{c_o^{(1)} \sqrt{n}} \mathcal{E}_{2,\infty,n}^{(2)} \right).$$

Thus, assumption of Theorem 3 implies that, for n large enough and any absolute constant $C_{K,\text{small}}$

$$\|\Xi(i, :)\| \leq \frac{\sqrt{K_1 K_2}}{n} C_{K,\text{small}}, \quad (\text{A43})$$

where $C_{K,\text{small}}$ is a small positive constant to be chosen later. From Equations (A41) and (A43), obtain that

$$\begin{aligned} \|e_i^\top (\widehat{U} - UW_U)\| &\leq C_\tau \left(\|\Xi(i, :)\| \frac{\sqrt{K_1 K_2} \sqrt{n}}{\sqrt{K}} + \frac{\sqrt{K_1 K_2}}{\sqrt{n}} (\mathcal{E}_{0,n}^{(1)} + \mathcal{E}_{1,n}^{(2)}) \right) \\ &\leq C_\tau \frac{\sqrt{K}}{\sqrt{n}} \left[\left(\frac{K_1 K_2}{K} C_{K,\text{small}} + \frac{\sqrt{K_1 K_2}}{\sqrt{K}} (\mathcal{E}_{0,n}^{(1)} + \mathcal{E}_{0,n}^{(2)}) \right) \right] \\ &\leq \frac{\sqrt{K}}{2\sqrt{2}C_o\sqrt{n}}, \end{aligned} \quad (\text{A44})$$

once n is sufficiently large, and assuming a suitably small choice of $C_{K,\text{small}}$. This implies that condition (A29) holds for any $i \in [n]$, so Theorem 3 has been proved.

Now, we finish the proof of Theorem 2. Let

$$\mathcal{J}_n^{(v)} \equiv \mathcal{J}_n^{(v)}(C_{\text{small}}) = \left\{ i \in [n] : \|\Xi^{(v)}(i, :)\| > \frac{C_{\text{small}}\sqrt{K_v}}{\sqrt{n}} \right\}, \quad v = 1, 2, \quad (\text{A45})$$

and

$$\mathcal{E}_n^{(v)} = |\mathcal{J}_n^{(v)}|, \quad v = 1, 2. \quad (\text{A46})$$

If $i \in (\mathcal{J}_n^{(1)})^c \cap (\mathcal{J}_n^{(2)})^c$, then by (A42), the bound (A43) holds, and row i is clustered correctly by condition (A29) and the inequality (A44). Denote

$$\mathcal{J}_n = \mathcal{J}_n^{(1)} \cup \mathcal{J}_n^{(2)}, \quad \mathcal{J}_n^c = (\mathcal{J}_n^{(1)})^c \cap (\mathcal{J}_n^{(2)})^c$$

Then,

$$\mathcal{E}_n = |\mathcal{J}_n| \leq \mathcal{E}_n^{(1)} + \mathcal{E}_n^{(2)}. \quad (\text{A47})$$

By Assumption 4,

$$\mathbb{P} \left\{ \|\Xi^{(v)}\|_F^2 \leq C_\tau K_v (\mathcal{E}_{0,n}^{(v)})^2 \right\} \geq 1 - n^{-\tau}. \quad (\text{A48})$$

and by the conditions of Theorem 2 and Assumption 2, one has

$$K_v (\mathcal{E}_{0n}^{(v)})^2 = o(1), \quad \text{as } n \rightarrow \infty. \quad (\text{A49})$$

Then, (A45) yields

$$\|\Xi^{(v)}\|_F^2 = \sum_{i=1}^n \|\Xi^{(v)}(i, :)\|^2 \geq \sum_{i \in \mathcal{J}_n^{(v)}} \|\Xi^{(v)}(i, :)\|^2 \geq \frac{K_v}{n} |\mathcal{J}_n^{(v)}| C_{\text{small}}^2. \quad (\text{A50})$$

Hence, (A48), (A49) and (A50) imply that

$$\mathbb{P} \left\{ \frac{\mathcal{E}_n^{(v)}}{n} \leq \frac{C_\tau}{C_{\text{small}}^2} (\mathcal{E}_{0,n}^{(v)})^2 \right\} \geq 1 - n^{-\tau}.$$

Therefore, due to (A47),

$$\mathbb{P} \left\{ \frac{\mathcal{E}_n}{n} \leq \frac{C_\tau}{C_{\text{small}}^2} \left[(\mathcal{E}_{0n}^{(1)})^2 + (\mathcal{E}_{0n}^{(2)})^2 \right] \right\} \geq 1 - 2n^{-\tau}. \quad (\text{A51})$$

Hence, $\mathcal{E}_n/n \rightarrow 0$ as $n \rightarrow \infty$ with high probability, and clustering is consistent.

A.3. Proof of Theorem 5

Let, as in the proof of Theorem 1, $\widehat{X} = \widehat{Z}^{(1,2)} = \widehat{Z}^{(1)} \circledast \widehat{Z}^{(2)}$ and $X = ZH^\top$. Then, it follows from (A3) and (A4) that

$$\sigma_K(X) \geq \frac{c_o \sqrt{n}}{\sqrt{K}}, \quad \|\widehat{X} - X\| \leq \sqrt{2(\mathcal{E}_{1,n} + \mathcal{E}_{2,n})}.$$

Observe that, by (A5), one has

$$\sigma_K(\widehat{X}) \geq \frac{c_o \sqrt{n}}{\sqrt{K}} \left(1 - \frac{\sqrt{2K}}{c_o} \frac{\sqrt{\mathcal{E}_{1n} + \mathcal{E}_{2n}}}{\sqrt{n}} \right). \quad (\text{A52})$$

In addition, for $1 \leq j \leq K_1 K_2 - K$,

$$\sigma_{K+j}(\widehat{X}) \leq \sigma_{K+j}(X) + \|\widehat{X} - X\| \leq \frac{c_o \sqrt{n}}{\sqrt{K}} \frac{\sqrt{2K}}{c_o} \frac{\sqrt{\mathcal{E}_{1n} + \mathcal{E}_{2n}}}{\sqrt{n}}. \quad (\text{A53})$$

Then, (20) and (21) follow directly from (A52) and (A53). If clustering is consistent and Assumptions 1, 2, 3 hold, then $K = O(1)$, $n^{-1} K (\mathcal{E}_{1n} + \mathcal{E}_{2n}) = o(1)$, so the theorem is valid.

A.4. Proof of Theorem 6

Let, as in the proof of Theorems 2 and 3,

$$X = U^{(1,2)} W_U^{(1,2)} = (U^{(1)} \circledast U^{(2)}) W_U^{(1,2)} = U D H^\top W_U^{(1,2)}, \quad \widehat{X} = \widehat{U}^{(1,2)} = \widehat{U}^{(1)} \circledast \widehat{U}^{(2)}$$

and $\Xi = \widehat{X} - X$. Recall that by (A23),

$$\sigma_K(X) \geq \frac{c_D \sqrt{K}}{\sqrt{K_1 K_2 n}}, \quad \sigma_{K+1}(X) = 0.$$

In addition, it follows from (A31) that, under Assumptions 1, 2, 4, and 5, with high probability

$$\sigma_K(\widehat{X}) \geq \frac{c_D \sqrt{K}}{\sqrt{K_1 K_2 n}} \left(1 - \frac{\widetilde{C}_\tau K_1 K_2 (\mathcal{E}_{0,n}^{(1)} + \mathcal{E}_{0,n}^{(2)})}{c_D \sqrt{K}} \right).$$

Moreover, by (A26), one has

$$\|\Xi\|_F \leq \frac{\widetilde{C}_\tau \sqrt{K_1} \sqrt{K_2}}{\sqrt{n}} (\mathcal{E}_{0,n}^{(1)} + \mathcal{E}_{0,n}^{(2)}).$$

Then, validity of the theorem follows from the fact that $\sigma_{K+j}(\widehat{X}) \leq \|\Xi\|$ for $j \geq 1$.

A.5. Proof of Hierarchical Clustering results

In this section, we prove that complete-linkage hierarchical clustering applied to the rows of $\widehat{U} = \text{SVD}_K(\widehat{U}^{(1)} \circledast \widehat{U}^{(2)})$ yields perfect clustering under the conditions of Theorem 3, and that the merge heights exhibit an elbow at step $n - K + 2$. Algorithm 3 shows the complete-linkage hierarchical clustering procedure.

Proof of Theorem 4: Let us first describe the strategy to the proof. In hierarchical clustering with complete linkage, we begin with n clusters each containing a single point, and at each merge, the number of clusters decreases by 1. Suppose the radius of the set of points belonging to each true cluster is less than the separation between true clusters. Then when points belong to the same true cluster, we expect the merge heights to be small, and only once all of the possible within-cluster merges have occurred will a merge bring together points that belong to distinct true clusters. This will happen at step $n - K + 1$, since at that step there will be $n - (n - K + 1) = K - 1$ clusters, necessitating that one contains points from multiple true clusters, and we will see a jump in the merge heights at this step. Now let us prove these claims.

Let $\mathcal{G}^{(t)}$ denote the partition obtained after t merges, and let $G_i^{(t)}$ denote the i -th cluster in this partition. When merging two clusters, there are two cases. First, if all of the points in the two clusters $G_i^{(t-1)}, G_j^{(t-1)}$ belong to the same true cluster, then for any $a \in G_i^{(t-1)}$ and $b \in G_j^{(t-1)}$ we have $z(a) = z(b)$. Hence, $e_a^\top UW_U = e_b^\top UW_U$, so

$$\|(e_a^\top - e_b^\top)\widehat{U}\| \leq \|e_a^\top(\widehat{U} - UW_U)\| + \|e_b^\top(\widehat{U} - UW_U)\| \leq 2\|\widehat{U} - UW_U\|_{2,\infty} \quad (\text{A54})$$

$$d(G_i^{(t-1)}, G_j^{(t-1)}) = \max\{\|\widehat{U}(a, \cdot) - \widehat{U}(b, \cdot)\| : a \in G_i^{(t-1)}, b \in G_j^{(t-1)}\} \leq 2\|\widehat{U} - UW_U\|_{2,\infty} \quad (\text{A55})$$

Second, if points in $G_i^{(t-1)} \cup G_j^{(t-1)}$ belong to at least two different true clusters, then there are some indices a and b in this union such that $z(a) \neq z(b)$. We have

$$\begin{aligned} \|(e_a^\top - e_b^\top)\widehat{U}\| &\geq \|(e_a^\top - e_b^\top)UW_U\| - \|(e_a^\top - e_b^\top)(\widehat{U} - UW_U)\| \\ &\geq \|(e_a^\top - e_b^\top)UW_U\| - 2\|\widehat{U} - UW_U\|_{2,\infty} \end{aligned} \quad (\text{A56})$$

Letting $s = \min_{z(i) \neq z(j)} \|U(i, \cdot) - U(j, \cdot)\|$, we have

$$\|(e_a^\top - e_b^\top)\widehat{U}\| \geq s - 2\|\widehat{U} - UW_U\|_{2,\infty} \quad (\text{A57})$$

Equation (A19) states that $s \geq \frac{\sqrt{2K}}{C_o\sqrt{n}}$. On the other hand, if we fix $\eta \in (0, 1/6)$, then choosing an even smaller constant $C_{K,\text{small}}$ in Equation (A43) if necessary, we can obtain the following upper bound from Equation (A44), which holds with high probability for large n :

$$\|\widehat{U} - UW_U\|_{2,\infty} \leq \eta \frac{\sqrt{2K}}{C_o\sqrt{n}} \leq \eta s. \quad (\text{A58})$$

This implies all of the initial merges are within-cluster, with merge heights $h(t) \leq 2\|\widehat{U} - UW_U\|_{2,\infty}$. At the t -th stage of the algorithm, there are $n - t + 1$ clusters. Therefore, at the $n - K + 1$ step, there are exactly K distinct clusters, and

$$h(n - K + 1) \leq 2\|\widehat{U} - UW_U\|_{2,\infty}. \quad (\text{A59})$$

So $G^{(n-K+1)}$ gives the exact cluster labels. This completes the proof of Theorem 4.

When we have access to \widehat{U} from Algorithm 1, we see that for subsequent steps $t \geq n - K + 2$, any merge must involve points from different true clusters, yielding

$$h(t) \geq s - 2\|\widehat{U} - UW_U\|_{2,\infty}. \quad (\text{A60})$$

Hence, a gap occurs in the merge heights at step $n - K + 2$, which separates within-cluster merges from between-cluster merges and ensures exact recovery. Combining Equations (A58), (A59), and (A60), we have

$$\begin{aligned} h(n - K + 2) - h(n - K + 1) &\geq (1 - 2\eta) \frac{\sqrt{2K}}{C_o\sqrt{n}} \\ h(k + 1) - h(k) &\leq 2\eta \frac{\sqrt{2K}}{C_o\sqrt{n}} \end{aligned}$$

for $k \leq n - K$. So there is an elbow in the merge heights when we apply Algorithm 3 to \widehat{U} , but this requires knowledge of K in order to choose the dimension of \widehat{U} . To address this issue, we consider applying Algorithm 3 to $\widehat{U}^{(1,2)}$ directly. This leads to Theorem 7, which we now prove.

Proof of Theorem 7: Let $s = \min_{z^{(i)} \neq z^{(j)}} \|U^{(1,2)}(i, :) - U^{(1,2)}(j, :)\|$. By Assumption 1, we have

$$s = \min_{z^{(i)} \neq z^{(j)}} \left(\frac{1}{n_{z_1^{(i)}}^{(1)} n_{z_2^{(i)}}^{(2)}} + \frac{1}{n_{z_1^{(j)}}^{(1)} n_{z_2^{(j)}}^{(2)}} \right)^{1/2} \geq \frac{\sqrt{2K_1 K_2}}{c_o^{(1)} c_o^{(2)} n}. \quad (\text{A61})$$

Recall that $\Xi = \widehat{U}^{(1,2)} - U^{(1,2)} W_U^{(1,2)}$, and for large n , Equation (A43) provides the high-probability bound

$$\|\Xi\|_{2,\infty} \leq \frac{\sqrt{K_1 K_2}}{n} C_{K,\text{small}}.$$

Let $\eta \in (0, 1/6)$. Then choosing a smaller value of $C_{K,\text{small}}$ if necessary, we can ensure that for large n , with high probability,

$$\|\Xi\|_{2,\infty} \leq \eta \frac{\sqrt{2K_1 K_2}}{c_o^{(1)} c_o^{(2)} n}.$$

Putting this together, the first $n - K + 1$ merges are within-cluster, with merge heights

$$h(t) \leq 2\|\Xi\|_{2,\infty} \leq 2\eta \frac{\sqrt{2K_1 K_2}}{c_o^{(1)} c_o^{(2)} n},$$

and all subsequent merges involve points from different true clusters, which must have heights

$$h(t) \geq s - 2\|\Xi\|_{2,\infty} \geq (1 - 2\eta) \frac{\sqrt{2K_1 K_2}}{c_o^{(1)} c_o^{(2)} n}.$$

These inequalities together prove Theorem 7.

Figure 12 illustrates the idea that a gap occurs in the merge heights at step $n - K + 2$. In both subfigures ($n = 1000$ and $K = 5$), a clear jump is observed between steps 996 and 997.

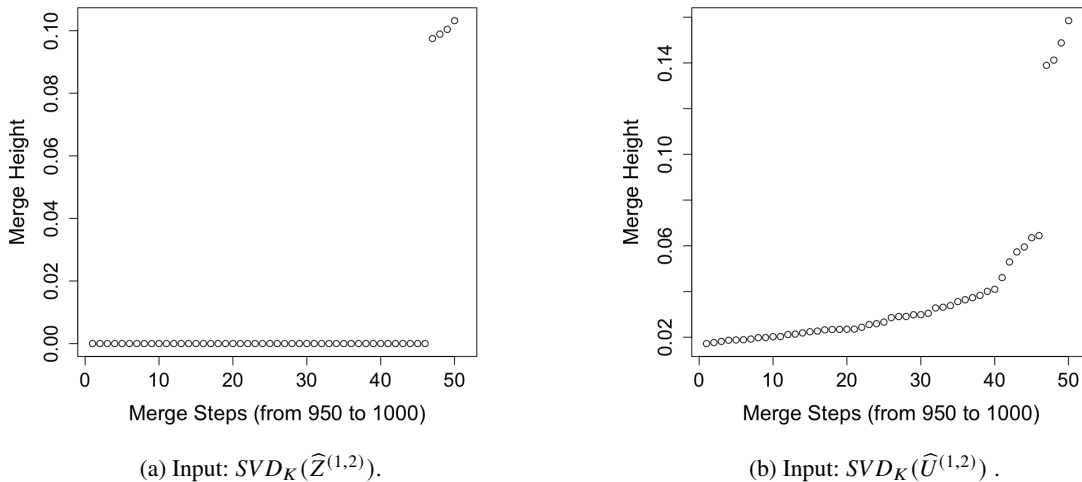


Fig. 12: Merge height plot for complete-linkage hierarchical clustering with $n = 1000$, $K = 5$, $K_1 = K_2 = 4$, $m = 30$, and $\sigma^2 = 0.25$.

A.6. Properties of the Khatri-Rao product and their proofs

- P1.** $(AC) \circledast (BD) = (A \circledast B)(C \otimes D)$.
P2. $\|A \circledast B\|_F \leq \min(\|A\|_F \|B\|_{2,\infty}, \|A\|_{2,\infty} \|B\|_F)$.

Proof:

$$\begin{aligned}
\|A \circledast B\|_F^2 &= \sum_{i=1}^n \|A(i, :) \otimes B(i, :)\|_2^2 \\
&= \sum_{i=1}^n [A(i, :) \otimes B(i, :)] [A(i, :) \otimes B(i, :)]^\top \\
&= \sum_{i=1}^n [A(i, :) A(i, :)]^\top \otimes [B(i, :) B(i, :)]^\top \\
&\leq \max_j \|A(j, :)\|^2 \sum_{i=1}^n \|B(i, :)\|^2; \text{ or} \\
&\leq \max_j \|B(j, :)\|^2 \sum_{i=1}^n \|A(i, :)\|^2.
\end{aligned}$$

- P3.** $\|A \circledast B\|_{2,\infty} \leq \|A\|_{2,\infty} \|B\|_{2,\infty}$.

Proof:

$$\begin{aligned}
\|A \circledast B\|_{2,\infty}^2 &= \max_i \|A(i, :) \otimes B(i, :)\|_2^2 \\
&= \max_i \|A(i, :)\|^2 \cdot \|B(i, :)\|^2 \\
&\leq \max_i \|A(i, :)\|^2 \cdot \max_v \|B(v, :)\|^2.
\end{aligned}$$

- P4.** $(A \circledast B)^\top = A^\top * B^\top$, where $A^\top * B^\top$ is the Khatri-Rao (columnwise) product.
P5. $(A \circledast B)(A^\top * B^\top) = (AA^\top) \circ (BB^\top)$ where $(X_1 \circ X_2)$ is the Hadamard product of X_1 and X_2 .
P6. $\|A \circledast B\| \leq \|A \otimes B\| = \|A\| \|B\|$.
P7. If $Z^{(v)} \in \{0, 1\}^{n \times K_v}$, $v = 1, 2$, are clustering matrices, then $Z^{(1)} \circledast Z^{(2)} \in \{0, 1\}^{n \times K_1 K_2}$ and $(Z^{(1)} \circledast Z^{(2)})^\top (Z^{(1)} \circledast Z^{(2)}) = \mathcal{D}_Z^{(1,2)}$ is a diagonal matrix with elements

$$\mathcal{D}_{Z, (k_1, k_2)}^{(1,2)} = \sum_{i=1}^n I(i \in \mathcal{G}_{k_1}^{(1)}) \cdot I(i \in \mathcal{G}_{k_2}^{(2)}) = n_{(k_1, k_2)}^{(1,2)},$$

where $\mathcal{G}_{k_v}^{(v)}$, $v = 1, 2$, is the group k_v according to clustering $v \in \{1, 2\}$, $k_v \in [K_v]$.

Proof: Consider $\mathcal{L} = (Z^{(1)} \circledast Z^{(2)})^\top (Z^{(1)} \circledast Z^{(2)}) \in \mathbb{R}^{K_1 K_2 \times K_1 K_2}$. Then, using double-indexing, one can write

$$\begin{aligned}
\mathcal{L}((k_1, k_2), (\tilde{k}_1, \tilde{k}_2)) &= \sum_{i=1}^n \left(Z^{(1)} \circledast Z^{(2)} \right) (i, (k_1, k_2)) \left(Z^{(1)} \circledast Z^{(2)} \right) (i, (\tilde{k}_1, \tilde{k}_2)) \\
&= \sum_{i=1}^n I(i \in \mathcal{G}_{k_1}^{(1)}) I(i \in \mathcal{G}_{k_2}^{(2)}) I(i \in \mathcal{G}_{\tilde{k}_1}^{(1)}) I(i \in \mathcal{G}_{\tilde{k}_2}^{(2)}) \\
&= \sum_{i=1}^n I(i \in \mathcal{G}_{k_1}^{(1)}) I(i \in \mathcal{G}_{k_2}^{(2)}) I(k_1 = \tilde{k}_1, k_2 = \tilde{k}_2) \\
&= n_{(k_1, k_2)}^{(1,2)}
\end{aligned}$$

B. VISUAL COMPARISON OF $\widehat{U}^{(v)}$ AND $\widehat{Z}^{(v)}$ INPUTS

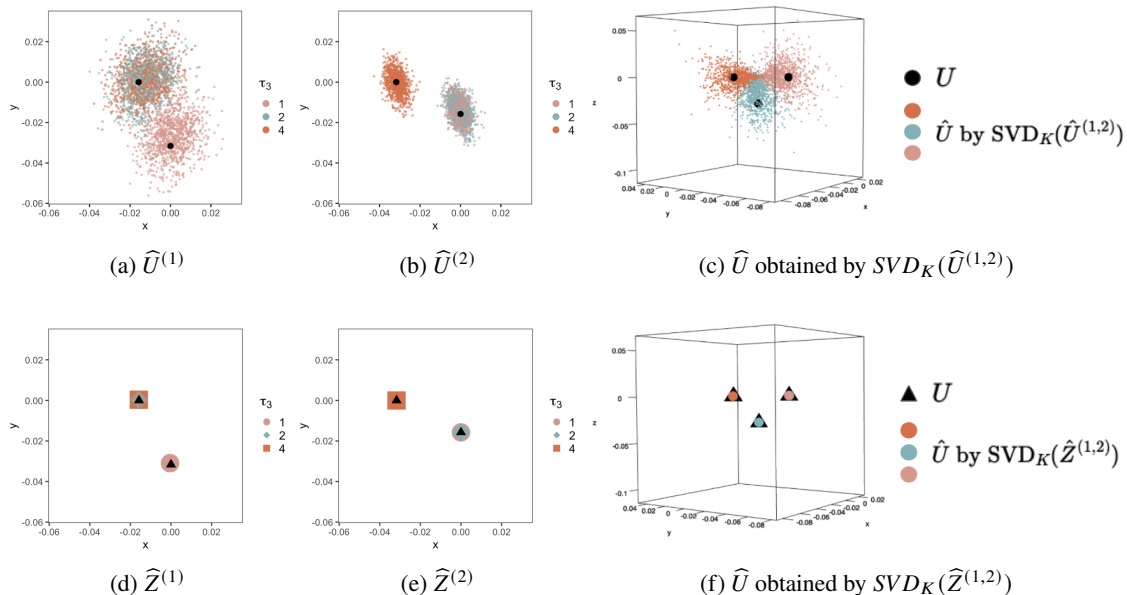


Fig. 13: Illustration of KRAFTY using simulated Gaussian mixtures with dimension $p = 3$ and $K = 3$ joint clusters. (a) $\widehat{U}^{(1)}$ from View 1; (b) $\widehat{U}^{(2)}$ from View 2; (c) left singular vectors from the SVD of $\widehat{U}^{(1)} \otimes \widehat{U}^{(2)}$. Bottom row: (d) $\widehat{Z}^{(1)}$ from View 1, scaled by the square root of singular values, with clustering obtained by k -means on $\widehat{U}^{(1)}$; (e) analogous results for $\widehat{Z}^{(2)}$ from View 2 using $\widehat{U}^{(2)}$; (f) left singular vectors from the SVD of $\widehat{Z}^{(1)} \otimes \widehat{Z}^{(2)}$. Points are colored by ground truth membership; black markers indicate the true cluster centers. We can observe that while three joint clusters exist, only two are distinguishable in each single view due to overlap. The figure conveys the idea that both $\widehat{U}^{(v)}$ and $\widehat{Z}^{(v)}$ target the same true centers; however, $\widehat{Z}^{(v)}$ collapses points toward centroids, while $\widehat{U}^{(v)}$ preserves the variance ‘cloud.’ The resulting \widehat{U} from either $\widehat{U}^{(v)}$ inputs or $\widehat{Z}^{(v)}$ inputs estimates the same U for the joint view. The joint space separates all clusters into orthogonal dimensions.

C. ADDITIONAL SIMULATION RESULTS

This section presents extended simulation results across three settings: varying the number of joint clusters, signal-to-noise ratios, and single-view cluster numbers.

C.1. Varying Number of Joint Clusters

Figure 14 compares MASE and KR for three joint cluster sizes $K \in \{4, 9, 15\}$ across varying noise levels σ^2 (x-axis). The number of clusters in each view are both 4 ($K_1 = K_2 = 4$), the dimension of the observations is $p = 20$, and this value is unchanged in the whole subsection. The top row uses $\widehat{Z}^{(v)}$ as input; the bottom row uses $\widehat{U}^{(v)}$. First, focusing on the results with $\widehat{Z}^{(v)}$ as input, when $K = 4 < K_1 + K_2$, MASE and KR perform similarly whether K is known or unknown. When $K > K_1 + K_2$ (i.e., $K = 9, 15$), MASE with known K and KR with known or unknown K achieve similar performance, all outperforming MASE with unknown K . This supports the finding that KR’s advantage comes from correctly estimating K .

For the U input (bottom row), when $K < K_1 + K_2$, MASE outperforms KR when K is unknown, while the two methods perform similarly when K is known. When $K > K_1 + K_2$, MASE and KR perform

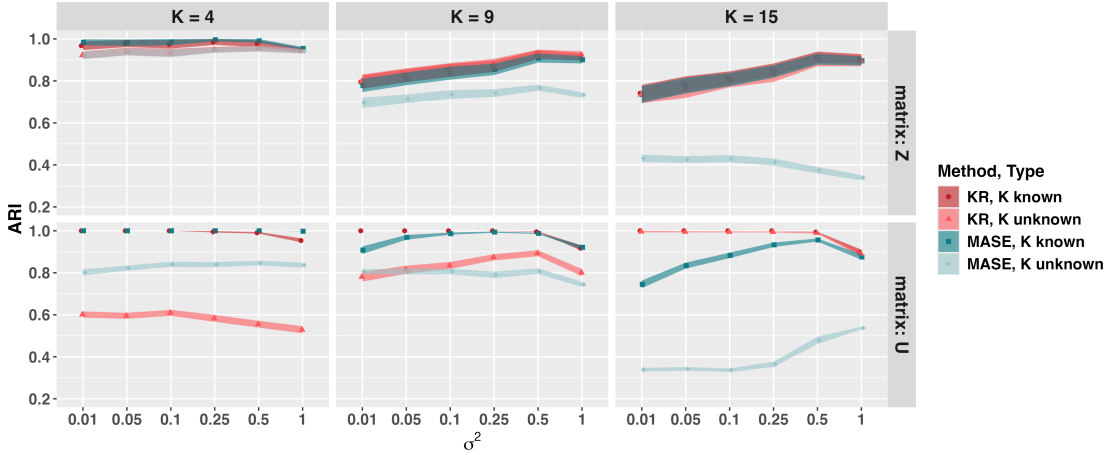


Fig. 14: Joint clustering performance of KR and MASE using $\widehat{Z}^{(v)}$ or $\widehat{U}^{(v)}$ matrices, evaluated under known and unknown K . The true number of joint clusters K is fixed at 4, 9, and 15, while the noise level σ^2 varies. ARI compares estimated joint clusters with ground truth. $K_1 = K_2 = 4$, $p = 20$.

similarly when K is known, but if K is unknown, there is a large performance gap between KR and MASE.

Figures 15 and 16 investigate how different inputs ($\widehat{Z}^{(v)}$ versus $\widehat{U}^{(v)}$) affect the performance of MASE and KR when the number of joint clusters K is unknown. In Figure 15, joint clustering performance (measured by ARI) is evaluated with noise levels fixed at either 0.01 or 1, while K varies from 4 to 16. We observe that when $K > K_1 + K_2$, MASE generally exhibits poor performance. However, under low noise conditions, $\widehat{Z}^{(v)}$ outperforms $\widehat{U}^{(v)}$ as K increases, whereas under high noise conditions, the opposite occurs ($\widehat{U}^{(v)}$ outperforms $\widehat{Z}^{(v)}$). KR's performance with different inputs also varies on different combinations of noise and number of joint clusters. $\widehat{U}^{(v)}$ outperforms $\widehat{Z}^{(v)}$ under low noise conditions, whereas $\widehat{Z}^{(v)}$ outperforms $\widehat{U}^{(v)}$ under high noise conditions when $K > K_1 + K_2$. Figure 16 presents a heatmap illustrating performance in estimating K when varying K and σ^2 simultaneously. The color represents the difference in Mean Absolute Error (MAE) for estimating K between the two inputs (calculated as $\text{MAE}_Z - \text{MAE}_U$). Consequently, cool colors indicate that $\widehat{Z}^{(v)}$ yields better performance (lower error), while warm colors indicate that $\widehat{U}^{(v)}$ is better. The results show that for MASE, $\widehat{U}^{(v)}$ and $\widehat{Z}^{(v)}$ has negligible difference. For KR, $\widehat{Z}^{(v)}$ yields better results at low levels of K and σ^2 ; however, this trend reverses as both parameters increase, with $\widehat{U}^{(v)}$ eventually outperforming $\widehat{Z}^{(v)}$.

C.2. Varying Signal-to-Noise Ratios

Figure 17 presents heatmaps illustrating how the performance of KR and MASE changes as dimensions and noise levels vary. The color scale represents the difference in ARI ($\text{ARI}_{\text{KR}} - \text{ARI}_{\text{MASE}}$); thus, cool colors indicate that MASE performs better, while warm colors indicate that KR performs better. In the known K setting (first two columns), inputs $\widehat{Z}^{(v)}$ yield similar results for both methods regardless the change of dimensions and noise levels. For inputs $\widehat{U}^{(v)}$, MASE is preferred when $K < K_1 + K_2$, while KR performs better when $K > K_1 + K_2$ under high signal-to-noise ratios. In the unknown K setting, for $\widehat{U}^{(v)}$, MASE is preferred when K is small. When $K = 12$ and signal-to-noise ratios are high, KR is better. Notably, when using $\widehat{Z}^{(v)}$, KR consistently outperforms MASE across all signal-to-noise ratios for both K is small or large. We conduct a similar comparison between the \widehat{U} and \widehat{Z} methods for KR and MASE in Figure 18.

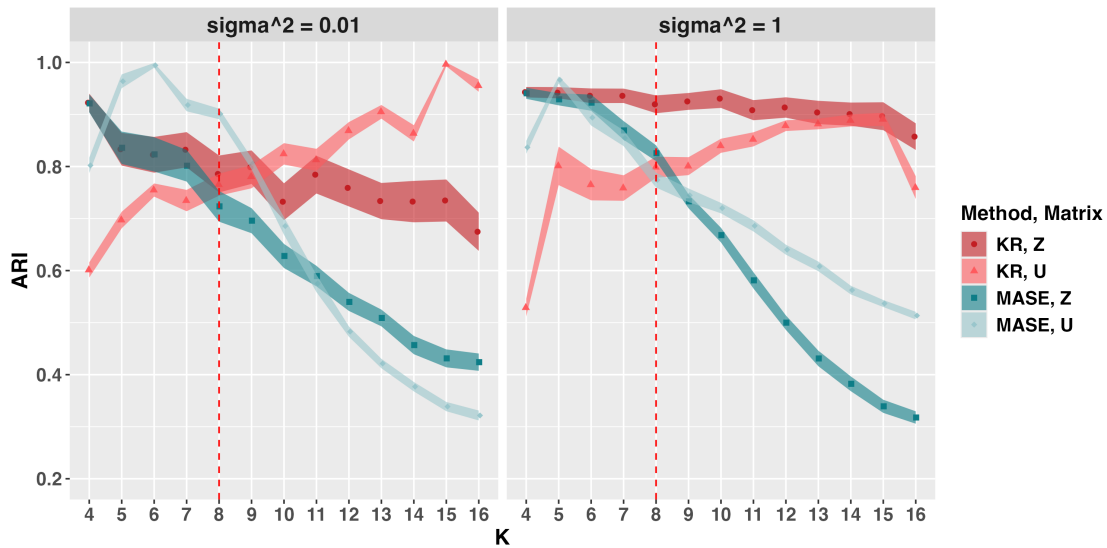


Fig. 15: Joint clustering performance across four combinations: KRAFTY with $\widehat{Z}^{(v)}$, KRAFTY with $\widehat{U}^{(v)}$, MASE with $\widehat{Z}^{(v)}$, and MASE with $\widehat{U}^{(v)}$, evaluated under the unknown K setting. The noise level σ^2 is set to either 0.01 or 1. ARI compares estimated joint clusters with ground truth. $K_1 = K_2 = 4, p = 20$.

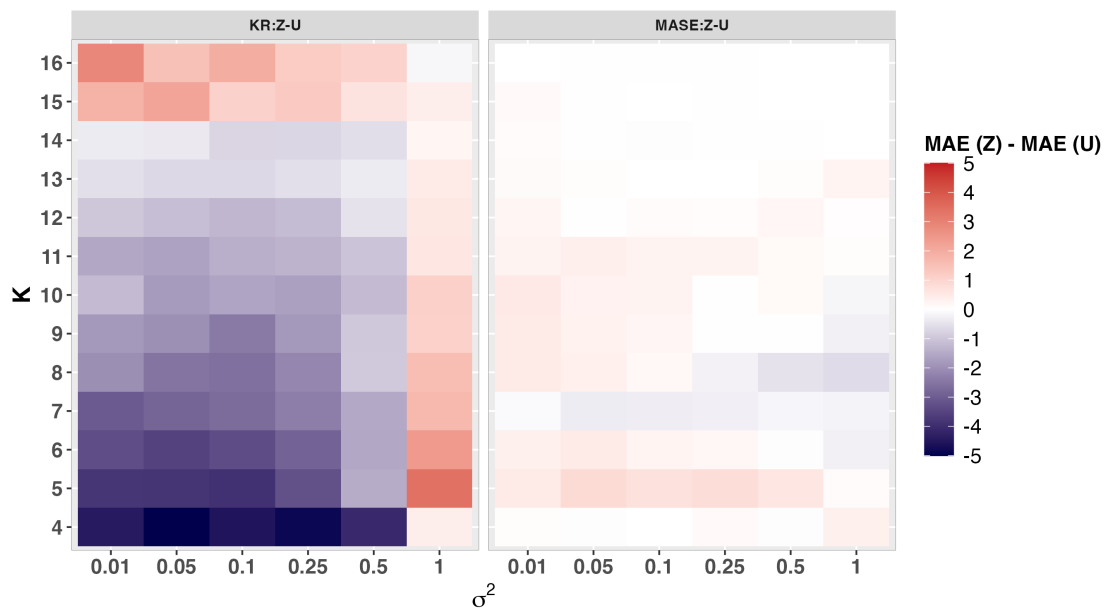


Fig. 16: Comparison of joint cluster number estimation performance between Z and U across KR and MASE methods. Heatmap colors represent the difference in mean absolute error (averaged over 100 repetitions) when estimating K using Z versus U. **Cool colors** \rightarrow **Z better**; **warm colors** \rightarrow **U better**. $K_1 = K_2 = 4, p = 20$.

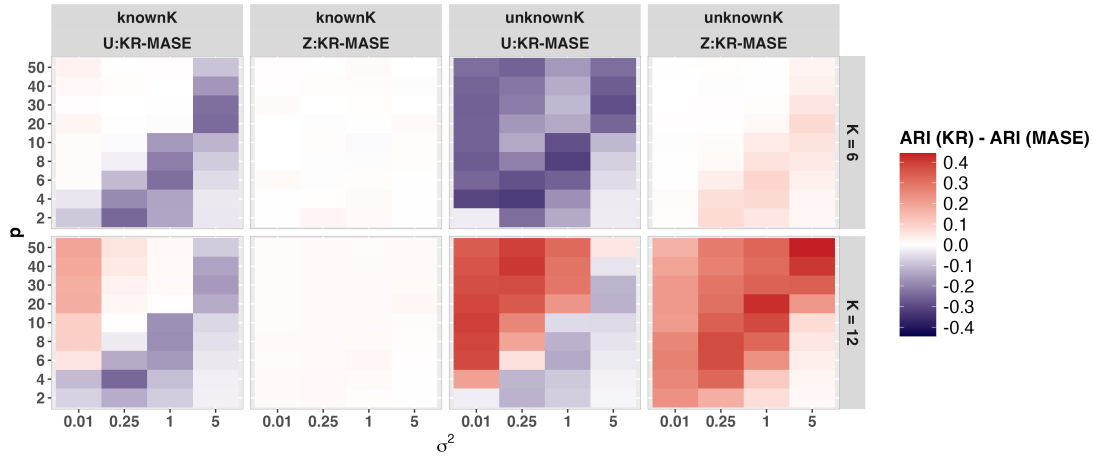


Fig. 17: Comparison of joint clustering performance between KR and MASE across Z and U matrices. The left 2 columns of the heatmap show the difference in mean ARI (averaged over 100 repetitions) between KR and MASE when the number of joint clusters K is **known**, using either the Z or U matrix. The right 2 columns show the difference in mean ARI between KR and MASE when K is **unknown**. **Cool colors** \rightarrow **MASE better**; **warm colors** \rightarrow **KR better**. $K_1 = K_2 = 4$.

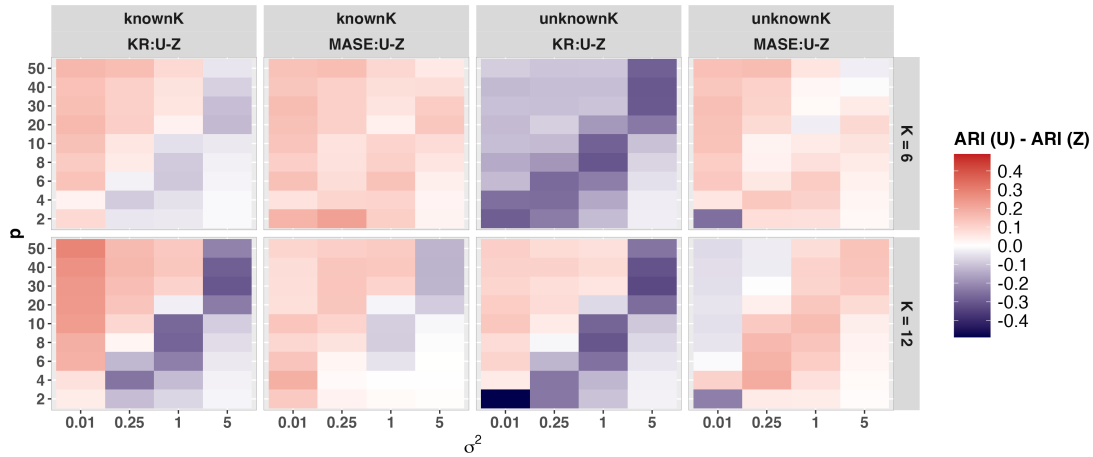


Fig. 18: Comparison of joint clustering performance between Z and U across KR and MASE methods. The left 2 columns of the heatmap show the difference in mean ARI (averaged over 100 repetitions) between Z and U when the number of joint clusters K is **known**, using either KR or MASE method. The right 2 columns show the difference in mean ARI between Z and U when K is **unknown**. **Cool colors** \rightarrow **Z better**; **warm colors** \rightarrow **U better**. $K_1 = K_2 = 4$.

C.3. Varying Number of Clusters in Single View

To obtain more robust conclusions, we conduct additional simulations where K_1 and K_2 vary from 3 to 10, and the true number of joint clusters K takes four representative values: two within the range of $K \leq K_1 + K_2$, specifically, $\max(K_1, K_2)$ and $K_1 + K_2$, two beyond that range, $\lfloor K_1 K_2 / 2 \rfloor$ and $K_1 K_2$. The noise level is fixed at $\sigma^2 = 0.1$ and the dimension at $p = 101$. The results are shown as heatmaps in Figures 19 and 20.

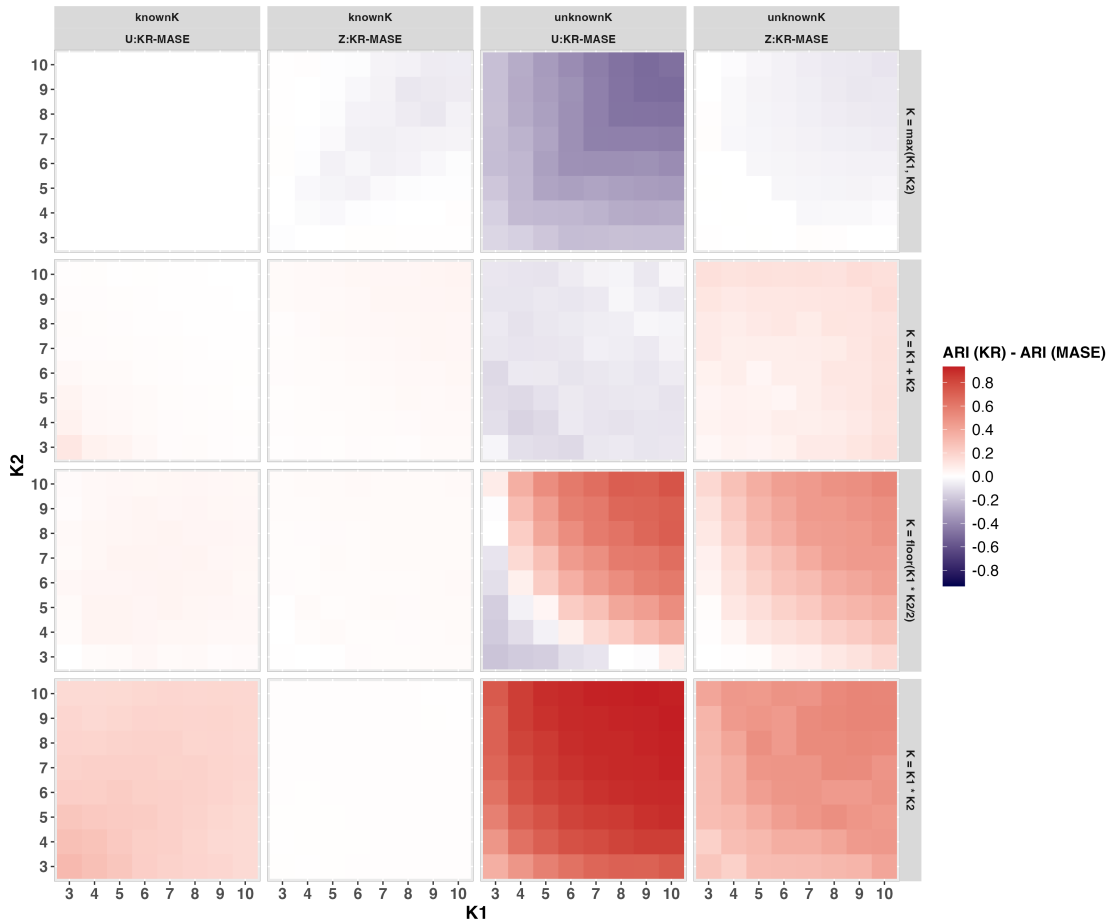


Fig. 19: Comparison of joint clustering performance between KR and MASE using Z and U matrices across 4 different true K settings, appearing in each row. The left 2 columns of the heatmap show the difference in mean ARI (averaged over 100 repetitions) between KR and MASE when the number of joint cluster K is **known**, using either the Z or U matrix. The right 2 columns show the difference in mean ARI between KR and MASE when K is **unknown**. **Cool colors** \rightarrow **MASE better**; **warm colors** \rightarrow **KR better**. $\sigma^2 = 0.1$, $p = 101$.

Figure 19 further corroborates that KRAFTY's advantage comes from its ability to correctly estimate K . In the left two columns (where K is known), the heatmaps are nearly white or light-colored, indicating that KRAFTY and MASE achieve similar joint clustering performance across various regimes governing the size of K . In contrast, the right two columns (where K is unknown) display more distinct warm colors as K increases, reflecting KRAFTY's improved performance.

Between the choices of using $\hat{Z}^{(v)}$ matrices and $\hat{U}^{(v)}$ matrices, the second right column in Figure 20 confirms that when K is small, KRAFTY with $\hat{Z}^{(v)}$ matrices yields better joint clustering performance, while when K is large, KRAFTY with $\hat{U}^{(v)}$ matrices performs better, as indicated by cool colors in the upper panels and warm colors in the lower panels.

Figure 21 illustrates the performance of estimating K under varying numbers of single-view clusters. Similar to the previous two figures, K_1 and K_2 range from 3 to 10, the dimension is fixed at 101, the noise level at $\sigma^2 = 0.1$, and the true K is defined according to: $\max(K_1, K_2)$, $K_1 + K_2$, $\lfloor K_1 K_2 / 2 \rfloor$, and $K_1 K_2$. The heatmap color represents the difference in Mean Absolute Error ($\text{MAE}_{\text{MASE}} - \text{MAE}_{\text{KR}}$); hence, cool colors

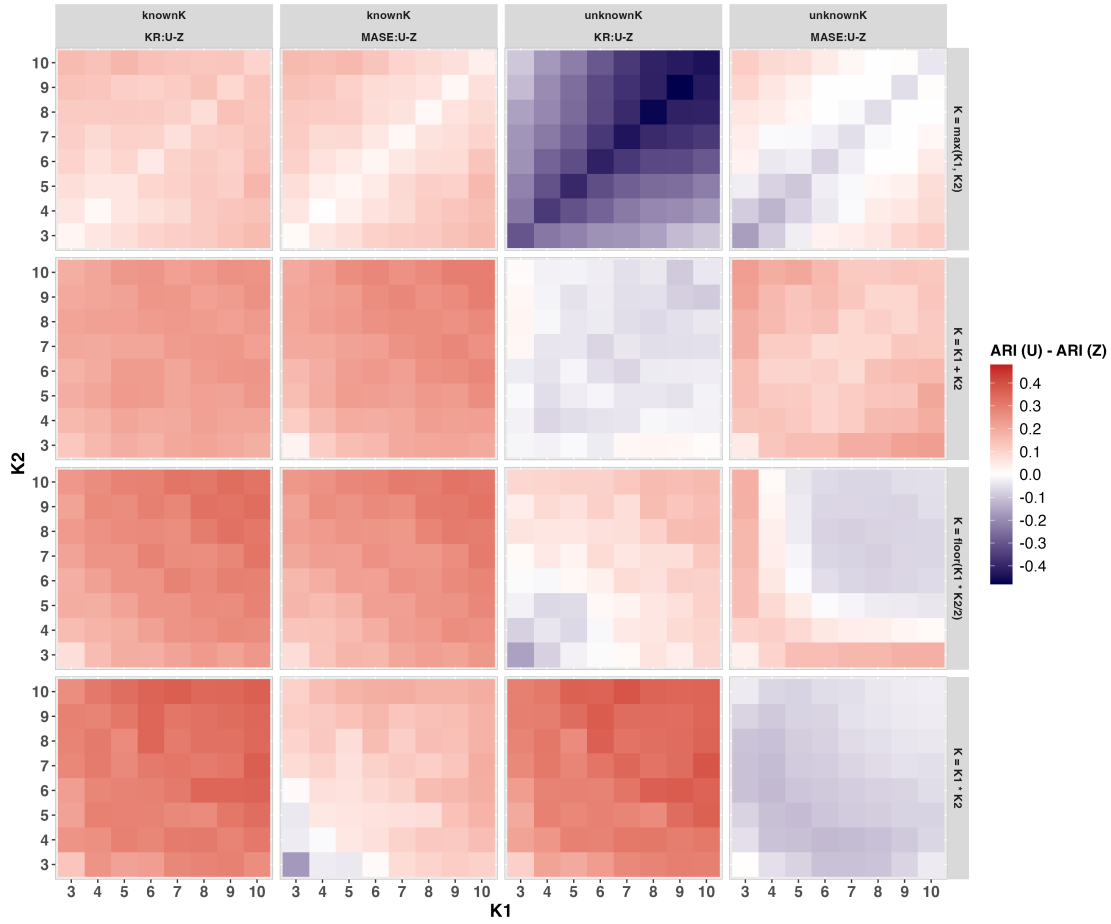


Fig. 20: Comparison of joint clustering performance between Z and U using KR or MASE across 4 different true K settings, appearing in each row. The left 2 columns of the heatmap show the difference in mean ARI (averaged over 100 repetitions) between U and Z when the number of joint cluster K is **known**, using either KR or MASE. The right 2 columns show the difference in mean ARI between U and Z when K is **unknown**. **Cool colors** \rightarrow Z better; **warm colors** \rightarrow U better. $\sigma = 0.1$, $p = 101$.

indicate that MASE is better and warm colors mean that KR is better. Under scenarios $K = \max(K_1, K_2)$ and $K = K_1 + K_2$, MASE generally outperforms KR since $K \leq K_1 + K_2$. However, in some cases when using $\hat{Z}^{(v)}$ as inputs, KR can achieve comparable performance. When $K > K_1 + K_2$, the advantage of KR becomes more pronounced as K increasingly exceeds $K_1 + K_2$.

Figure 22 illustrates the difference in performance of estimating K using \hat{Z} or \hat{U} as inputs ($\text{MAE}_Z - \text{MAE}_U$), across four true K settings. The top row (KR) and bottom row (MASE) show different behaviors. For MASE, the choice of input has negligible impact. For KR, however, patterns vary by setting: for $K \leq K_1 + K_2$, $\hat{Z}^{(v)}$ is preferred for small K , but $\hat{U}^{(v)}$ becomes better as K increases; for $K = K_1 K_2$, U is the better input. Conversely, in the $K = \lfloor K_1 K_2 / 2 \rfloor$ setting, $\hat{Z}^{(v)}$ yields lower errors specifically when $K < K_1 + K_2$.

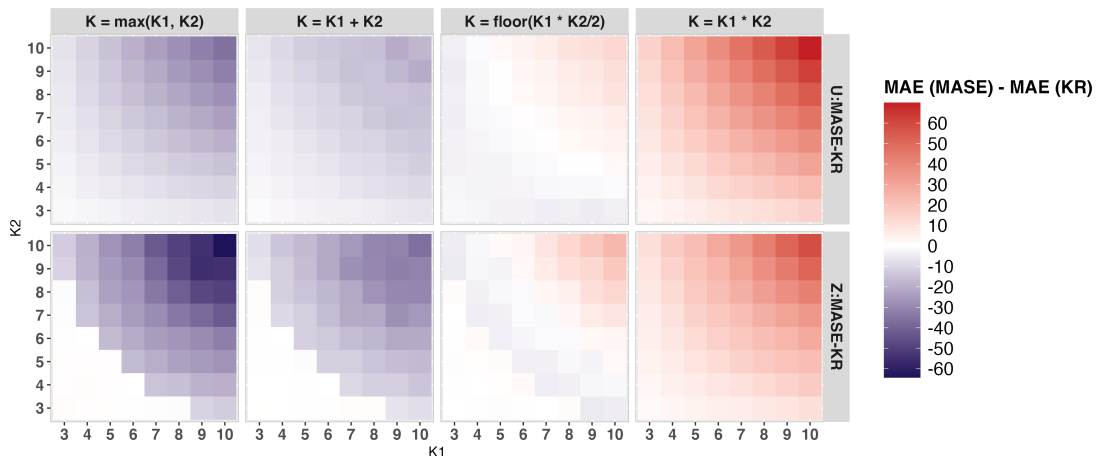


Fig. 21: Comparison of joint cluster number estimation performance between KR and MASE using Z or U matrices across 4 true K settings. The top row of the heatmap shows the difference in mean absolute error (averaged over 100 repetitions) between MASE and KR using U matrix. The bottom row shows the difference in mean absolute error between KR and MASE using Z matrix. **Cool colors** \rightarrow **MASE better**; **warm colors** \rightarrow **KR better**. $\sigma^2 = 0.1, p = 101$.

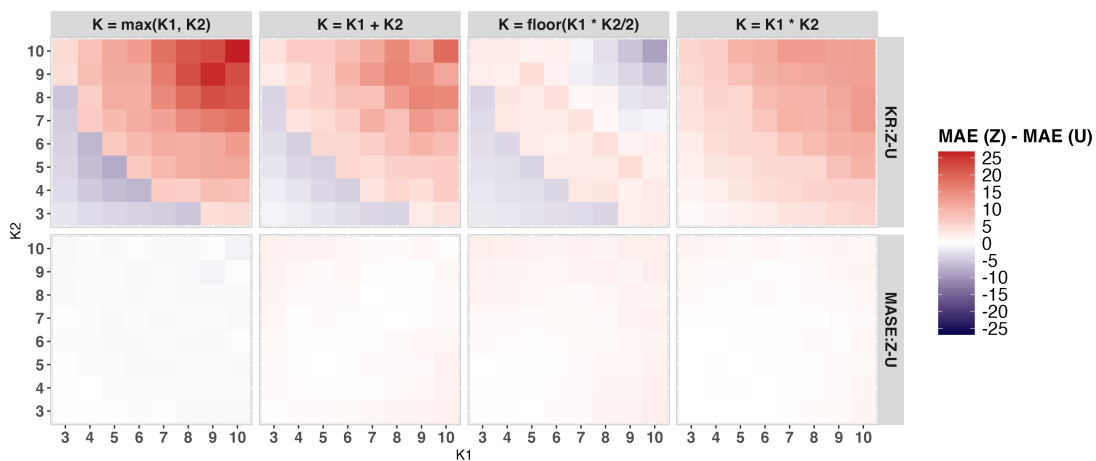


Fig. 22: Comparison of joint cluster number estimation performance between Z and U using KR or MASE across 4 different true K settings. The top row of the heatmap shows the difference in mean absolute error (averaged over 100 repetitions) when estimating K using Z versus U using KR. **Cool colors** \rightarrow **Z better**; **warm colors** \rightarrow **U better**. The bottom row shows the difference in mean absolute error between Z and U using MASE. $\sigma = 0.1, p = 101$.

C.4. Comparing X and U

This section demonstrates the performance similarity between $\hat{U}^{(v)}$ and its scaled counterpart $\hat{X}^{(v)} = \hat{U}^{(v)}(D^{(v)})^{1/2}$. Consistent with our previous analysis, we examine the same three experimental settings.

Varying Number of Joint Clusters

Figure 23 illustrates the performance as K varies at two noise levels. The results indicate that the choice between $\hat{X}^{(v)}$ and $\hat{U}^{(v)}$ has a negligible effect on joint clustering for both KR and MASE.

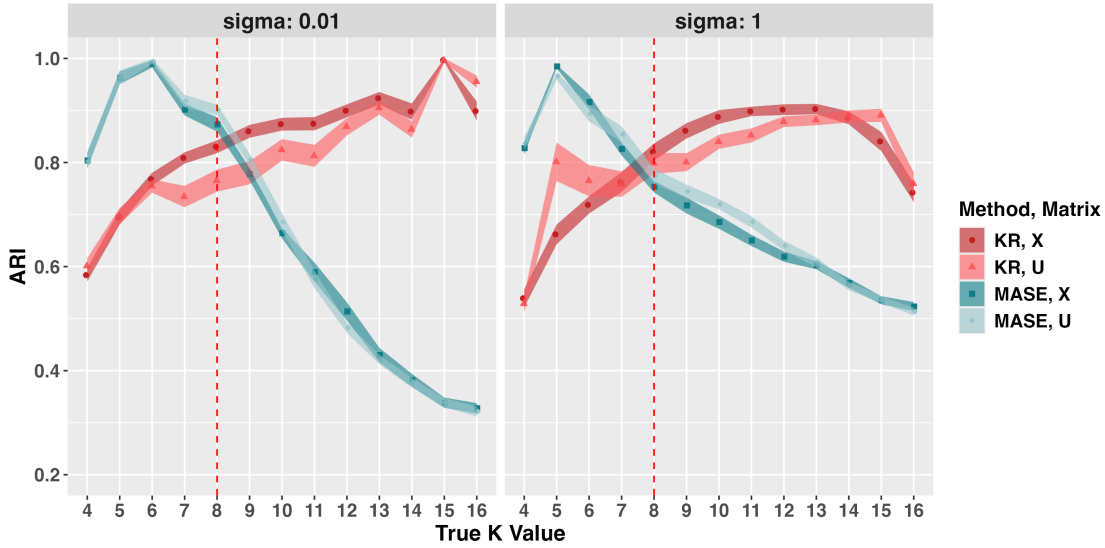


Fig. 23: Joint clustering performance of the X and U matrices using KR and MASE under **unknown** K setting. The noise level σ is set to either 0.01 or 1. ARI compares estimated joint clusters with ground truth. Here, $K_1 = K_2 = 4$, $p = 20$.

Figure 24 illustrates the performance as σ^2 varies for three different K scenarios. We observe that the lines representing $\hat{X}^{(v)}$ and $\hat{U}^{(v)}$ overlap. It indicates that the choice between these inputs has a negligible effect on the joint clustering performance of both KR and MASE.

Figure 25 displays the heatmap comparing the performance of inputs $\hat{X}^{(v)}$ and $\hat{U}^{(v)}$ in estimating K . The observed difference in error is negligible.

Varying Signal-to-Noise Ratio We compare the performance of inputs $\hat{U}^{(v)}$ and $\hat{X}^{(v)}$ in joint clustering (Figure 26) and in estimating K (Figure 27) when varying dimensions and noise levels. Consistent with previous findings, the performance discrepancies between the two inputs remain minimal.

Varying Number of Clusters in Single View We compare the performance of inputs $\hat{U}^{(v)}$ and $\hat{X}^{(v)}$ in joint clustering (Figure 28) and in estimating K (Figure 29), across varying single-view cluster numbers and four different K settings. Consistent with previous findings, the performance discrepancies between the two inputs remain negligible.

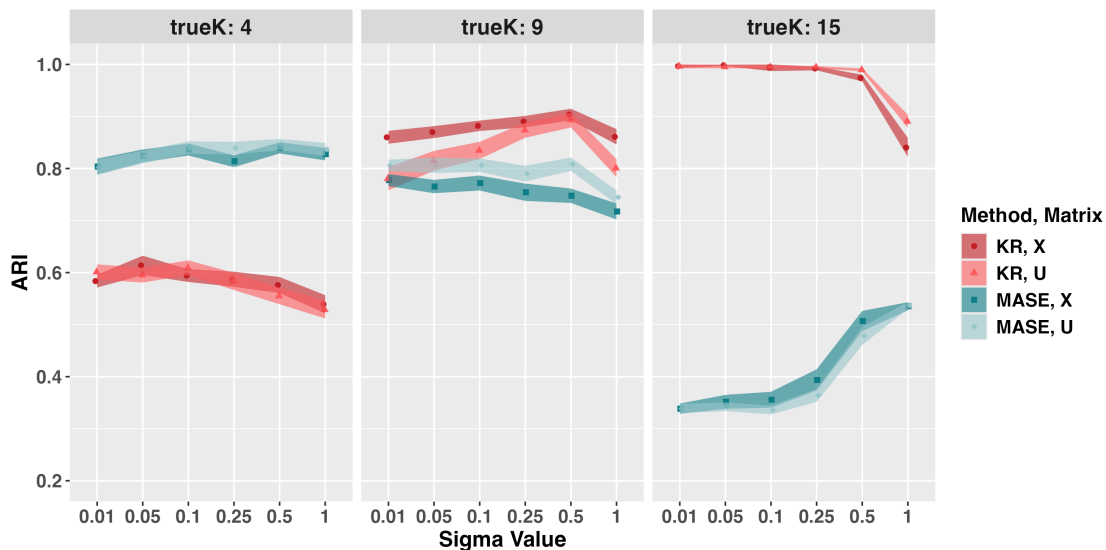


Fig. 24: Joint clustering performance of the X and U matrices using KR and MASE under **unknown** K setting. The true number of joint clusters K is held constant at 4, 9, and 15 across experiments, with σ varying. ARI compares estimated joint clusters with ground truth. Here, $K_1 = K_2 = 4$, $p = 20$.

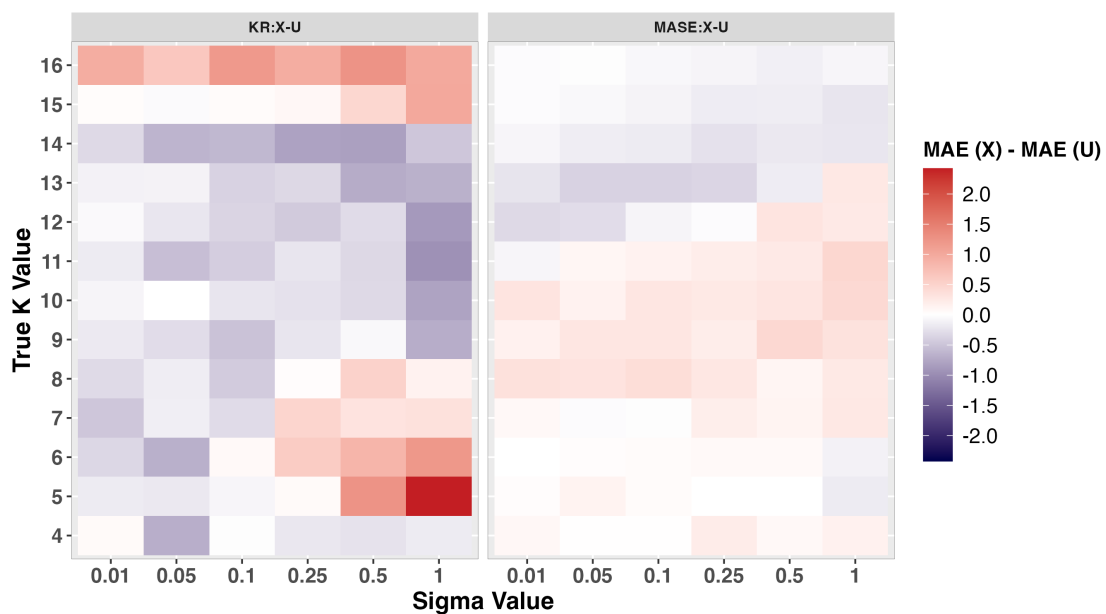


Fig. 25: Comparison of joint cluster number estimation performance between X and U across KR and MASE methods. Heatmap colors represent the difference in mean absolute error (averaged over 100 repetitions) when estimating K using X versus U. **Cool colors** \rightarrow X better; **warm colors** \rightarrow U better. $K_1 = K_2 = 4$, $p = 20$.

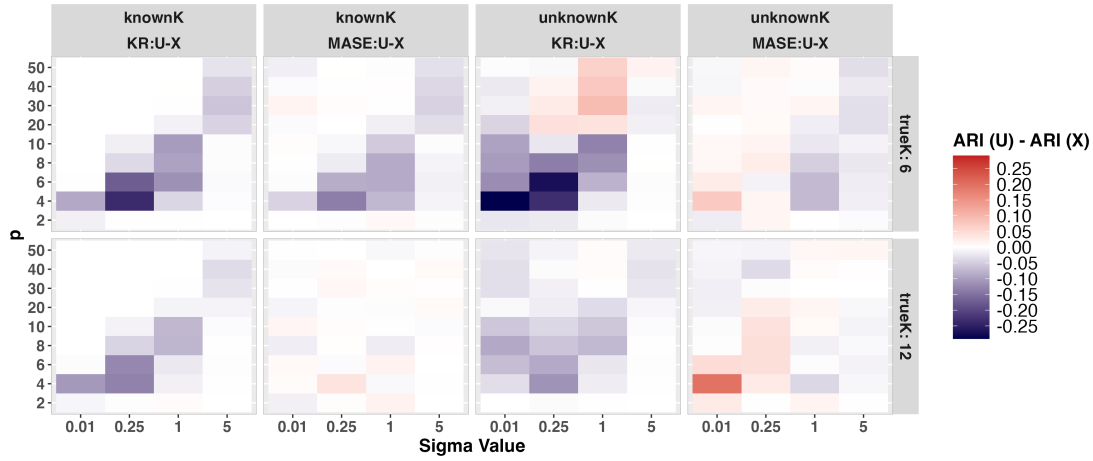


Fig. 26: Comparison of joint clustering performance between X and U across KR and MASE methods. The left 2 columns of the heatmap show the difference in mean ARI (averaged over 100 repetitions) between X and U when the number of joint clusters K is **known**, using either KR or MASE method. The right 2 columns show the difference in mean ARI between X and U when K is **unknown**. **Cool colors** \rightarrow X better; **warm colors** \rightarrow U better. $K_1 = K_2 = 4$.

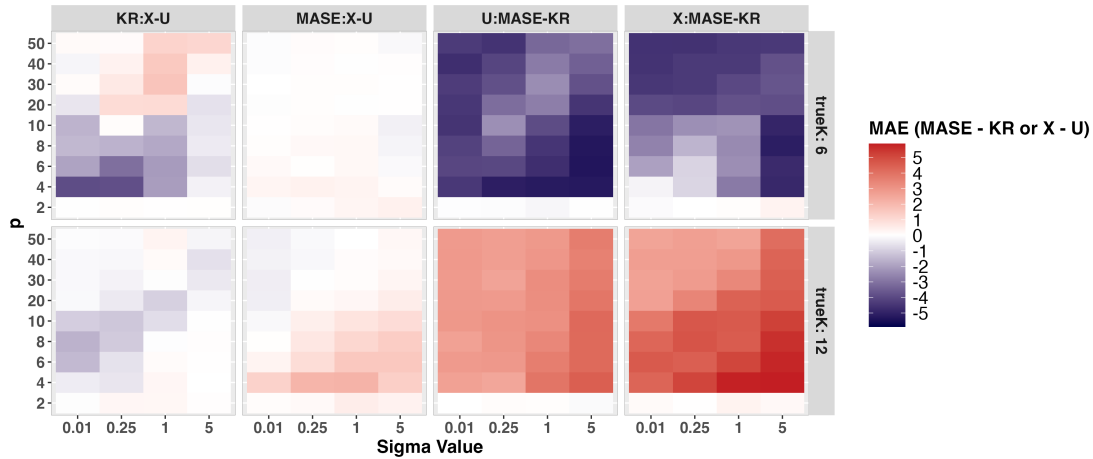


Fig. 27: Comparison of joint cluster number estimation performance between KR and MASE across X and U matrices. The left two columns of the heatmap show the difference in mean absolute error (averaged over 100 repetitions) when estimating K using X versus U. **Cool colors** \rightarrow X better; **warm colors** \rightarrow U better. The right 2 columns show the difference in mean absolute error between KR and MASE methods. **Cool colors** \rightarrow MASE better; **warm colors** \rightarrow KR better. Here, $K_1 = K_2 = 4$.

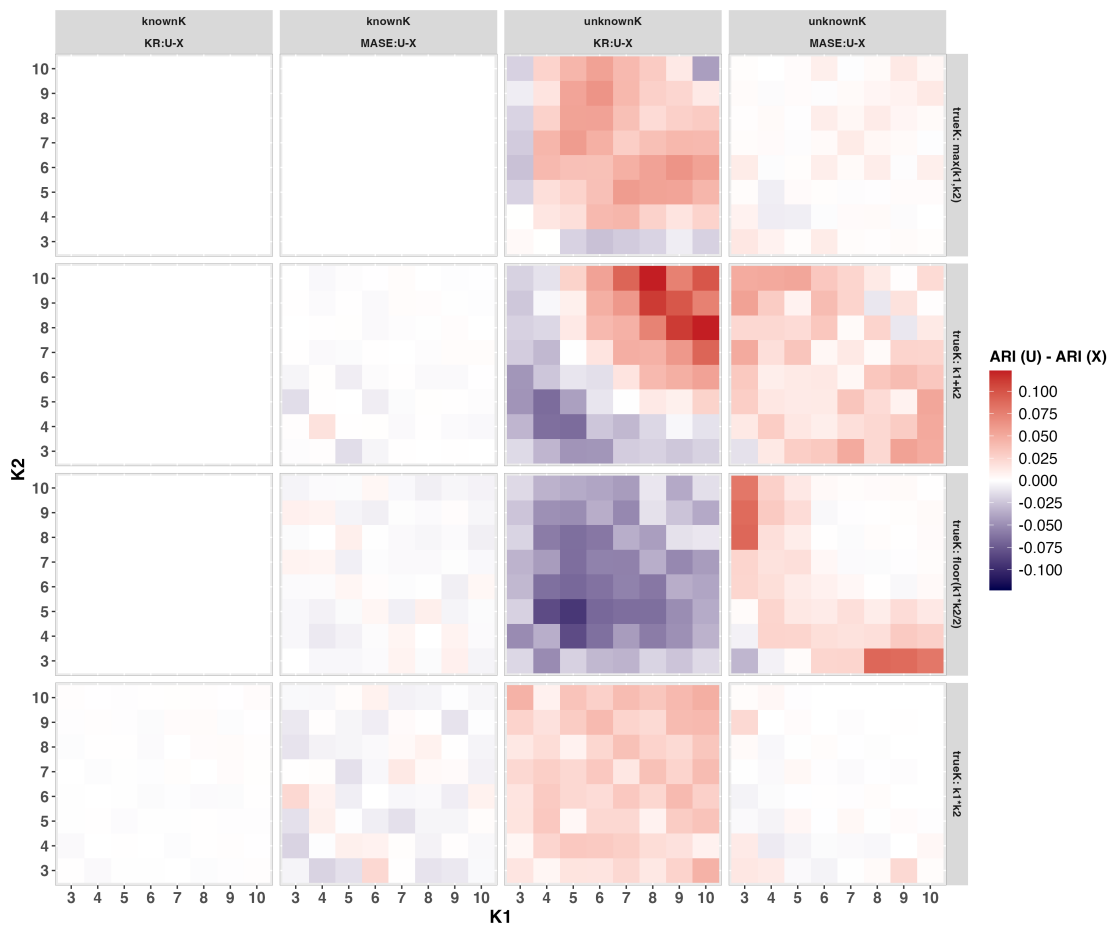


Fig. 28: Comparison of joint clustering performance between X and U using KR or MASE across 4 different true K settings. The left 2 columns of the heatmap show the difference in mean ARI (averaged over 100 repetitions) between U and X when the number of joint cluster K is **known**, using either KR or MASE. The right 2 columns show the difference in mean ARI between U and X when K is **unknown**. **Cool colors** \rightarrow **X better**; **warm colors** \rightarrow **U better**. $\sigma = 0.1$, $p = 101$.

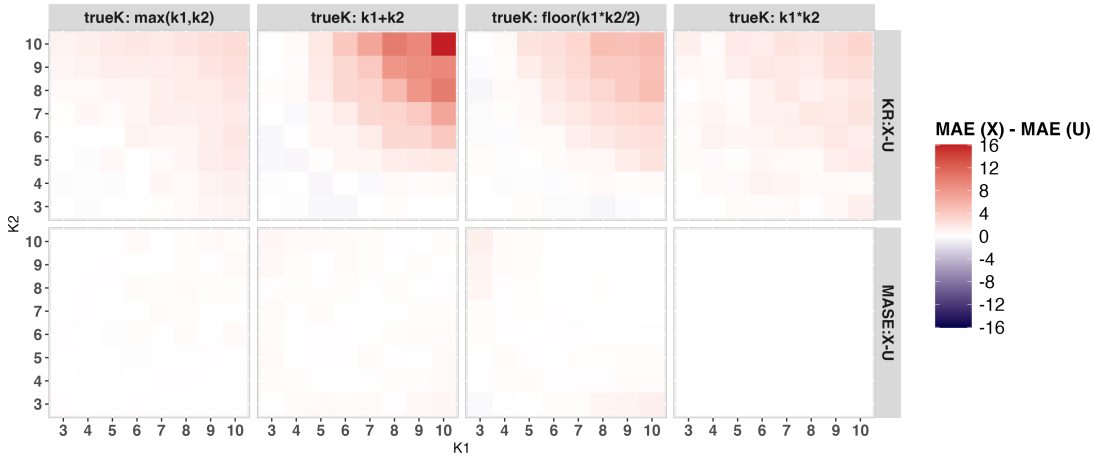


Fig. 29: Comparison of joint cluster number estimation performance between X and U using KR or MASE across 4 different true K settings. The top row of the heatmap shows the difference in mean absolute error (averaged over 100 repetitions) when estimating K using X versus U using KR. **Cool colors** \rightarrow X better; **warm colors** \rightarrow U better. The bottom row shows the difference in mean absolute error between X and U using MASE. $\sigma = 0.1, p = 101$.

D. REAL DATA ANALYSIS SUPPLEMENTARY

In this section, we provide supplementary figures for the real data analysis, along with the two-year analysis.

D.1. Single-year Results on Global Trade Data Analysis

Figure 30 presents the adjacency matrix for the raw chicken meat trade network. The matrix is symmetrized by summing the export and import volumes for each pair of countries. Rows and columns are ordered according to the clusters estimated by KRAFTY, arranged from Cluster 1 to Cluster 5 (consistent with the sequence in Figure 10). Notably, we observe that trading volume within Cluster 1 and Cluster 4 is small.

D.2. Two-year Results on Global Trade Data Analysis

We aim to identify time-invariant latent structure, i.e., the ‘unchanging’ clusters, among countries acting as exporters or importers. We apply KRAFTY and MASE to $\hat{Z}^{(v)}$ with $v \in \{(2010, \text{imp}), (2023, \text{exp})\}$ and $v \in \{(2010, \text{exp}), (2023, \text{exp})\}$. The results are shown in Figs. 31–38. The scree plots display a clear elbow under KRAFTY, which are consistent with our theory; moreover, KRAFTY and MASE yield highly consistent joint clusters (Fig. 35, 36), which aligns with our simulations. Comparing KRAFTY’s joint clusters to combinations of single-view clusters, we can see how the joint clusters are derived from the single-view partitions (Figs. 33, 34). One interpretation is that country-level export/import behavior shifts across years, leading to view-specific differences, while a stable joint structure persists.

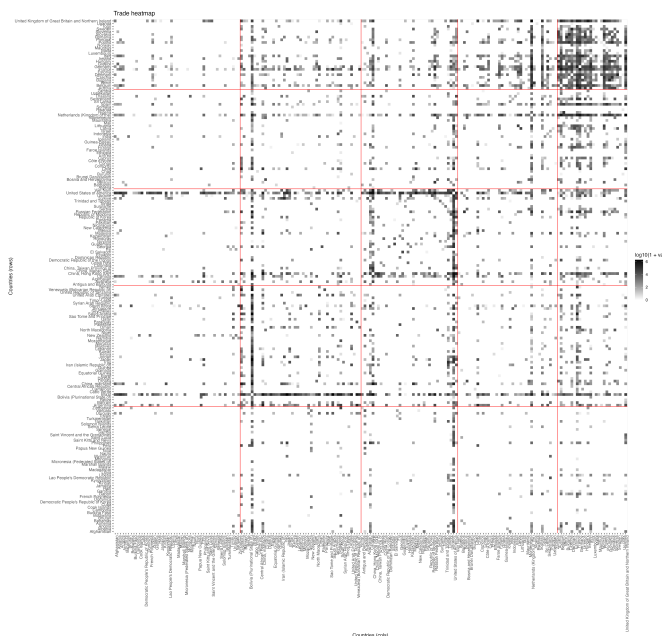


Fig. 30: Global trade adjacency heatmap; countries are sorted in KRAFTY joint clusters and boundaries are indicated by red lines.

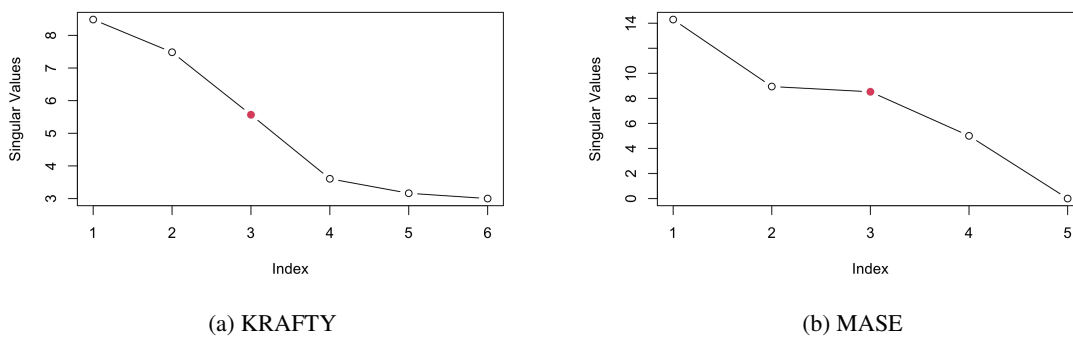


Fig. 31: Eigenvalue scree plot for two-year exporters only; the red dot indicates the selected dimension.

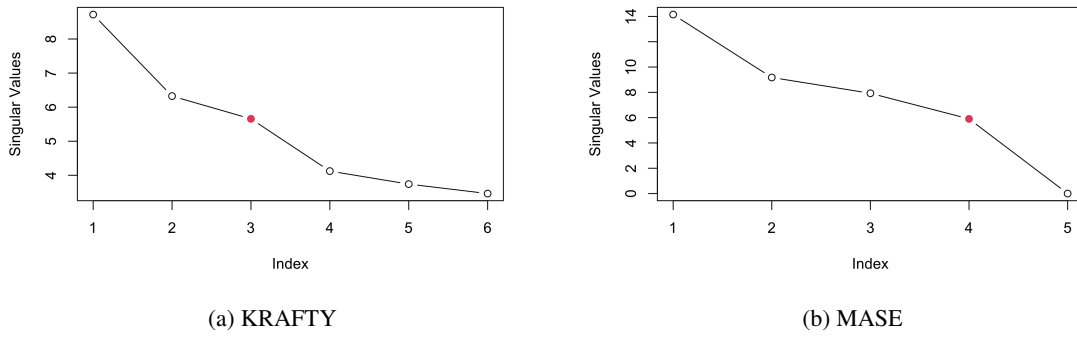


Fig. 32: Eigenvalue scree plot for two-year importers only; the red dot indicates the selected dimension.

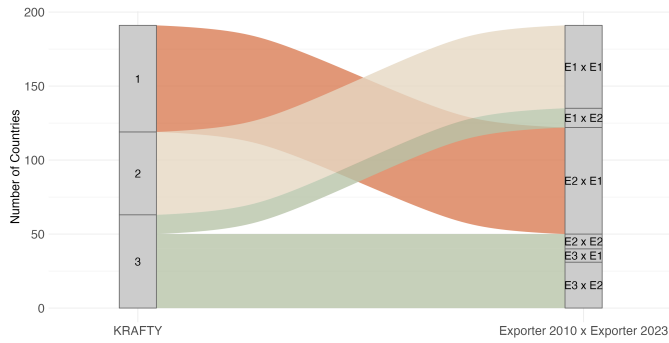


Fig. 33: Alluvial plot of joint clusters by KRAFTY vs. single-sourced clusters (exporters); identical colors indicate the same set of entities, and block height reflects the number of countries in each cluster.

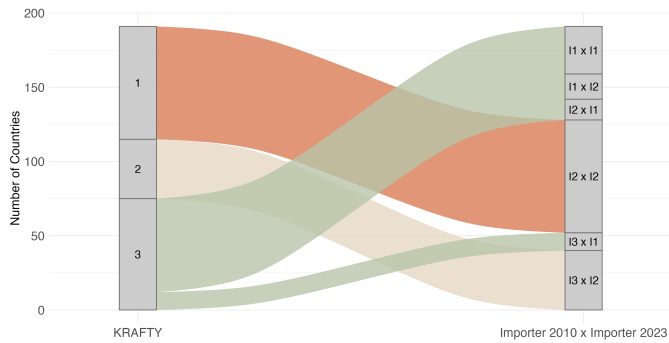


Fig. 34: Alluvial plot of joint clusters by KRAFTY vs single-sourced clusters (importers); identical colors indicate the same set of entities, and block height reflects the number of countries in each cluster.

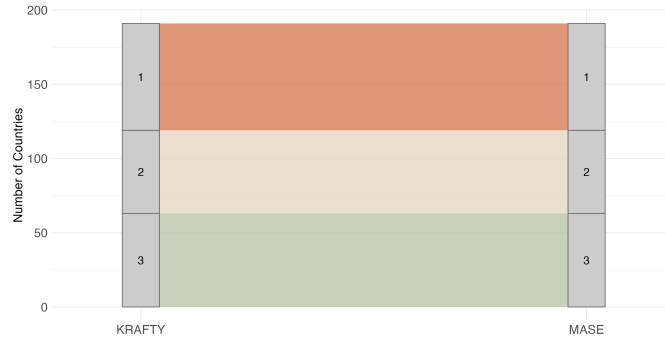


Fig. 35: Alluvial plot of Joint Clusters by KRAFTY vs by MASE (Exporters); identical colors indicate the same set of entities, and block height reflects the number of countries in each cluster.



Fig. 36: Alluvial plot of joint clusters by KRAFTY vs by MASE (importers); identical colors indicate the same set of entities, and block height reflects the number of countries in each cluster.



Fig. 37: World map colored by KRAFTY joint clusters for two-year exporters; blue color denotes cluster membership.



Fig. 38: World map colored by KRAFTY joint clusters for two-year importers; blue color denotes cluster membership.